AD-A251 647

DTIC
ELECTE
JUN 17 1992
S D
C

(2)

NONLINEAR GUIDED-WAVE PHENOMENA

Accesion For
NTIS CRA&I
DTIC TAB
Unannounced
Justification
By
Distribution /
Availability Codes
Dist Avail and / or Special
A-1

Sponsored by
Optical Society of America

POSTDEADLINE PAPERS

SEPTEMBER 2–4, 1991
CAMBRIDGE, ENGLAND
UNITED KINGDOM

92 6 15 169

92-15631

REPORT DOCUMENTATION PAGE

Form Approved
OMB No. 0704-0188

Public reporting burden for this collection of information is estimated to average 1 hour per response, including the time for reviewing instructions, searching existing data sources, gathering and maintaining the data needed, and completing and reviewing the collection of information. Send comments regarding this burden estimate or any other aspect of this collection of information, including suggestions for reducing this burden, to Washington Headquarters Services, Directorate for information Operations and Reports, 1215 Jefferson Davis Highway, Suite 1204, Arlington, VA 22202-4302, and to the Office of Management and Budget, Paperwork Reduction Project (0704-0188), Washington, DC 20503.

1. AGENCY USE ONLY (Leave blank)	2. REPORT DATE	3. REPORT TYPE AND DATES COVERED
	May 22, 1992	Final 1/1/91-12/31/91

4. TITLE AND SUBTITLE
Organization of the 1991 Optical Society of America Photonic Science Topical Meeting Series

5. FUNDING NUMBERS
G - AFOSR-91-0176

6. AUTHOR(S)
Jarus W. Quinn

7. PERFORMING ORGANIZATION NAME(S) AND ADDRESS(ES)
Optical Society of America
2010 Massachusetts Ave. NW
Washington, DC 20036

8. PERFORMING ORGANIZATION REPORT NUMBER
AFOSR-TR- 92 0510

9. SPONSORING/MONITORING AGENCY NAME(S) AND ADDRESS(ES)
US Air Force Office of Scientific Research
Department of the Air Force
Bolling Air Force Base
Washington, DC 20332-6448
NE
Schlossberg

10. SPONSORING/MONITORING AGENCY REPORT NUMBER
2305/A1

11. SUPPLEMENTARY NOTES

12a. DISTRIBUTION/AVAILABILITY STATEMENT
Approved for public release
Distribution unlimited

12b. DISTRIBUTION CODE

13. ABSTRACT (Maximum 200 words)

Attach list of reports supported by Optical Society of America
Photorefractive Materials, Effects, and Devices
Integrated Photonics Research
Nonlinear Guided Wave Phenomena
Optical Amplifiers and Their Applications
Optical computing
Picosecond Electronics and Optoelectronics
Quantum Optoelectronics
Photonic Switching
Microphysics of Surfaces: Beam Induced Processes
Soft X-ray Projection Lithography
Short Wavelength Coherent Radiation, Generation & Applications
Presistent Spectral Hole-Buring: Science & Applications

14. SUBJECT TERMS

15. NUMBER OF PAGES

16. PRICE CODE

17. SECURITY CLASSIFICATION OF REPORT	18. SECURITY CLASSIFICATION OF THIS PAGE	19. SECURITY CLASSIFICATION OF ABSTRACT	20. LIMITATION OF ABSTRACT

PDP-1 Monday, 10:30 AM

NONLINEAR MIXING OF OPTICAL SOLITONS WITH DIFFERENT FREQUENCES

V.V. Afanasjev and V.A. Vysloukh

Abstract

The problem of the mixing of one-soliton pulses with different carrying frequencies is considered. Parameters of solitons forming in far field zone is calculated by a method based on the Inverse Scattering Transform.

PDP-2 Tuesday, 9:00 PM

Nonlinear Directional Coupler in $Al_{0.18}Ga_{0.82}As$ Near Half the Band Gap.

J. S. Aitchison, A. H. Kean and C. N. Ironside,
Department of Electronics and Electrical Engineering,
University of Glasgow,
Glasgow, G12 8QQ

A. Villeneuve and G. I. Stegeman,
CREOL,
University of Central Florida,
Orlando, FL, 32826

Accession For
By
Distribution/
Availability Codes
Dist Avail and/or Special
A-1

Abstract:

We report the first experimental observation of an ultrafast all-optical switch in a semiconductor waveguide configuration where the transmission is not limited by absorption processes.

PDP-3 Tuesday, 9:10 PM

Nonlinearity Near Half-Gap in Bulk and Quantum Well GaAs/AlGaAs Waveguides

M.N. Islam,[a)] C.E. Soccolich,[a)] R.E. Slusher,[b)] A. F. J. Levi,[b)] W. S. Hobson,[b)] and M.G. Young [a)]

a) AT&T Bell Laboratories, Holmdel, NJ 07733
b) AT&T Bell Laboratories, Murray Hill, NJ 07974

phone: (908) 949-5428
fax: (908) 949-2473

ABSTRACT

We report the nonlinear index and two-photon absorption coefficient near half-gap in bulk and multiple quantum well GaAs/AlGaAs waveguides. Pump-probe measurements show an intriguing exchange of energy between orthogonal axes.

PDP-4 Tuesday, 9:20 PM

Field Dependent All-optical Switching in GaAs Quantum Well Waveguides operating beyond the Two Photon Absorption Limit

H.K.Tsang, R.V.Penty and I.H.White

University of Bath, School of Physics, Bath BA2 7AY, U.K.

R.S.Grant, W.Sibbett

University of St.Andrews, Dept. of Physics and Astronomy, St. Andrews KY16 9SS, U.K.

J.B.D.Soole, E.Colas, N.C.Andreadakis, H.P.LeBlanc

Bellcore, 331 Newman Springs Road, Red Bank NJ07701, USA.

Abstract

We report a field dependent two photon absorption in GaAs/AlGaAs multi-quantum well waveguides near half bandgap, and over π radians phase modulation from sub-picosecond nonlinear refraction.

PDP-5 Tuesday, 9:30 PM

SECOND HARMONIC GENERATION IN OPTICAL FIBRES - THE ROLE OF THE LONGITUDINAL FIELDS IN SYMMETRY BREAKING

Mark G Sceats and Simon B Poole

Optical Fibre Technology Centre
University of Sydney NSW 2046
Australia

ABSTRACT

Seeded SHG in fibres is quantitatively explained by the proposition that the longitudinal field of the pump mode is involved in the ionisation of Ge-Si wrong bonds through a 3-photon ionisation process invoving two pump photons and one seed photon. This interference produces a grating of defects which has the correct inversion asymmetry to produce SHG. Optical pumping of the trapped electrons in Ge(1) centres developes an electrostatic field which produces SHG by the EFISH mechanism.

PDP-6 Tuesday, 9:40 PM

Saturation of two-photon excited photoluminescence in Ge-doped fiber

Sophie LaRochelle, Alain Blouin, and François Ouellette

Université Laval

Centre d'Optique, Photonique et Lasers

Département de génie électrique

Québec (Québec), Canada, G1K 7P4

Abstract

The 400 nm photoluminescence band of Ge-doped optical fiber was excited by two-photon absorption of 488 nm and 514 nm cw argon laser light. We observed a saturation of the luminescence signal as the excitation light power was increased. From the measured value of the saturation intensity, and the luminescence lifetime, the two-photon absorption cross-section can be estimated.

PDP-7 Tuesday, 9:50 PM

Interference between photon echoes in an Er-doped fiber

V.L. da Silva, Y. Silberberg, J.P. Heritage, and E.W. Chase

Bellcore, 331 Newman Springs Road, Red Bank, New Jersey 07701-7040
Tel: (908) 758-3130, FAX: (908) 741-2891

Abstract

We report the observation of a new interference effect that leads to a near cancellation of the second order photon echo in an Er-doped fiber.

PDP-8 Tuesday, 10:00 PM

PASSIVE, ALL-FIBRE SOURCE OF FUNDAMENTAL, FEMTOSECOND SOLITONS

D.J.RICHARDSON, A.B. GRUDININ AND D.N. PAYNE

OPTOELECTRONICS RESEARCH CENTRE
UNIVERSITY OF SOUTHAMPTON
S09 5NH, UK

We report for the first time the generation of 50 fs solitons from an all-fibre circuit comprising a passively mode-locked erbium-doped fibre laser, an erbium-doped fibre amplifier and a short section of dispersion-shifted fibre.

PDP-9 Tuesday, 10:10 PM

Repetition rate control of an LD-pumped femtosecond erbium-doped fiber laser using a sub ring cavity

by

Masataka Nakazawa, Eiji Yoshida, and Yasuo Kimura
Nonlinear Optical Transmission Media Research Group
NTT Optical Transmission Line Laboratory
Tokai, Ibaraki-ken 319-11
Japan

Abstract

The pulse repetition rate of a femtosecond erbium-doped fiber laser with a nonlinear amplifying loop mirror can be controlled by attaching a sub ring linear cavity whose transit time is the inverse integer of that in the main cavity.

PDP-10 Tuesday, 10:20 PM

A Digital Nonlinear Optical Loop Mirror Switch

N. Finlayson, B.K. Nayar, N.J. Doran
BT Laboratories, Martlesham Heath, Ipswich

ABSTRACT

A novel double-pass nonlinear optical loop mirror is used to generate digital all-optical switching characteristics. The device is capable of generating square pulses.

PDP-11 Tuesday, 10:30 PM

All-optical, all-fiber circulating shift register with inverter

N. A. Whitaker, Jr., M. C. Gabriel, H. Avramopoulos, A. Huang
AT&T Bell Laboratories
Holmdel, NJ 07733

Abstract

An all-optical fiber-Sagnac interferometer switch and erbium amplifier have been combined to form a 254 bit circulating shift register with an inverter.

PDP-12 Tuesday, 10:40 PM

All-optical analog-to digital and digital-to-analog conversion based on cross-phase modulation

J.-M. Jeong and M. E. Marhic

Department of Electrical Engineering and Computer Science
Northwestern University
2145 Sheridan Rd., Evanston, Illinois 60208

Phone: (708) 491 7074
FAX: (708) 491 4455

Abstract

All-optical analog-to digital and digital-to analog converters using cross-phase modulation in a two-wavelength nonlinear interferometer are proposed and demonstrated.

NONLINEAR MIXING OF OPTICAL SOLITONS WITH DIFFERENT FREQUENCES

V.V. Afanasjev
Academy of Sciences of the USSR, General Physics Institute,
38 Vavilov street, 117942 Moscow, USSR
Telex 411074 LIMEN SU, Fax (7095) 135-8139,
Tel.(7095) 132-8306, E-mail serkin@sci.fian.msk.su (Internet)
V.A. Vysloukh
Moscow State University, Physics Department, 119899 Moscow, USSR
Telex 411483 MGU SU, Fax (7095) 939-3113, Tel. (7095) 939-3091

The subject of this work is results of theoretical investigation and computer simulations of nonlinear dynamics of wave packets, forming under mixing of optical solitons. The interest to this problem is motivated by the important application of solitons to spectral multiplexing in soliton communication systems and by possibility to use soliton effects in femtosecond laser systems in order to control the parameters of short light pulses.

In this work we consider the range of picosecond pulse duration, for which the complex envelope of electrical field $q(z,\tau)$ is described by Nonlinear Schrödinder equation (see, for example [1])

$$i\frac{\partial q}{\partial z} = \frac{1}{2}\frac{\partial^2 q}{\partial \tau^2} + |q|^2 q, \qquad (1)$$

where the distance z is expressed in units of dispersion length $L_d = \tau_0^2/|k_2|$, $\tau = (t - z/u)\tau_0^{-1}$ is moving time normalized to the initial pulse duration τ_0, u is the group velocity, $k_2 = \partial^2 k/\partial\omega^2$. The complex amplitude is normalized to the maximum value, corresponding to the amplitude of one-soliton pulse $|q_n| = [8\pi k_2/(\tau_0^2 k_0 n_2 c n_0)]^{1/2}$, where $k = k(\omega_0)$ is the propagation constant, n_0 - refractive index, n_2-nonlinear refractive index.

The one-soliton solution of (1) is

$$q_s = \kappa_0 \mathrm{sech}[\kappa_0(\tau - \tau_c - Vz)]\exp[i\theta(z,\tau)],$$
$$\theta(z,\tau) = -V_0\tau + (V_0^2 - \kappa_0^2)z/2 + \phi_0, \qquad (2)$$

where κ_0 is the soliton form-factor, defining the amplitude and duration of soliton, τ_c - is the coordinate of amplitude maximum, ϕ_0 - initial phase, V - soliton velocity (in this form of normalization V is equivalent to frequency detuning).

We are interested in the initial conditions in the form of superposition of two one-soliton pulses

$$q_0(\tau) = \mathrm{sech}(\tau_1)\exp[-i(p\tau_1 + \phi)] +$$
$$\mathrm{sech}(\tau_1)\exp[i(p\tau_2 + \phi)], \qquad (3)$$
$$\tau_1 = \tau + \tau_s,\ \tau_2 = \tau - \tau_s,$$

where parameter $p = \tau_0(\omega_2 - \omega_1)/2$ characterize the dimensionless frequency detuning between carrying frequencies ω_1 and ω_2, parameter τ_s is the initial time separation and ϕ — phase mismatch.

This problem was discussed recently in analogous mathematical statement in [2]. Authors of [2], using the Inverse Scattering Transform [3] analyse the case of great frequency mismatch ($p \gg 1$). The main result is that for great p, wave packet (2) divides into two solitons with equal amplitudes, and difference of velocities decreases by a value δV, which is proportional to p^{-2}. This result [2] is in a good agreement with the experimental data [4]. In this paper we discuss the case of small p ($p < 1$) by analytical approach; and in numerical experiments we discuss the wide range of p and the dynamics of transitional process.

Our purposes are to analyse the features of propagation of wave packets (2) and discuss the possibility of using the nonlinear interference effects for compression of pulses and control of the pulse carrying frequency.

Analytical approach It is known [3], that the forming soliton parameters may be obtained from the eigenvalues problem:

$$i\Phi + v\Phi = \Lambda\sigma\Phi,$$
$$\Phi = \begin{pmatrix}\Phi_1\\ \Phi_2\end{pmatrix},\ v = \begin{pmatrix}0 & q_0\\ q_0^* & 0\end{pmatrix},\ \sigma = \begin{pmatrix}1 & 0\\ 0 & -1\end{pmatrix}. \qquad (4)$$

where initial conditions (3) enter in the form of a potential. We rewrite (3) in the form

$$q_0(\tau) = N\mathrm{sech}(\tau) + \delta q(\tau), \quad (5)$$

where $N = 2$, and

$$\delta q(\tau) = N\mathrm{sech}[\cos(p\tau) - 1] \text{ at } \tau_c = 0,\ \phi = 0. \quad (6)$$

For $p < 1$, $\delta q(\tau)$ is the small perturbation

$$\delta q(\tau) \approx -p^2\mathrm{sech}(\tau). \quad (7)$$

It is known [5], that the initial conditions (5) at $p = 0$ (and, accordingly, at $\delta q = 0$), correspond to a N-soliton bound state with the form-factors $\kappa_m = 2m - 1$, where $m = 1, \ldots, N$ and the zero velocities $V_m = 0$. To analyse the influence of the perturbation δq on the parameters κ_m, V_m, we use the technique developed in [6] for arbitrary N. According to this technique, it is possible to present the perturbance parameters of m-soliton component (where $m = 1$ corresponds to a soliton with maximum form-factor) in an integral form:

$$\delta\kappa_m = \int_{-\infty}^{+\infty} K_S^m(\tau)\mathrm{Re}[\delta q(\tau)]d\tau,$$

$$\delta V_m = \int_{-\infty}^{+\infty} K_A^m(\tau)\mathrm{Im}[\delta q(\tau)]d\tau, \quad (8)$$

where a symmetric with respect to τ responce function K_S^m and an antisymmetric one K_A^m are expressed by the variational derivatives of eigenvalues of (4)

$$K_S^m = 2|\delta\Lambda_m/\delta q + \delta\Lambda_m/\delta q^*|,$$

$$K_A^m = 2|\delta\Lambda_m/\delta q - \delta\Lambda_m/\delta q^*|, \quad (9)$$

Formulas obtained in [6] for variational derivatives are

$$\frac{\delta\Lambda_m}{\delta q} = i\frac{\Gamma(2N - m + 1)}{\Gamma^2(N)[2\mathrm{ch}(\tau)]^{2N}} \times$$

$$\left[B_{m-2}^{N-1}(\tau)e^{\tau} + B_{m-1}^{N-1}(\tau)\right]^2 e^{\tau}d\tau, \quad (10)$$

and

$$\frac{\delta\Lambda_m}{\delta q^*}(\tau) = \frac{\delta\Lambda_m}{\delta q}(-\tau),$$

where Γ is the Gamma-function, and function B_n^{N-1} is determined from the expansion

$$[1+2\mathrm{sh}(\tau)y-y^2]^{N-1} = \sum_{n=0}^{2(N-1)} B_n^{N-1}(\tau)y^n,\ B_{-1}^{N-1} = 0. \quad (11)$$

From a comparison of (6) and (8), we obtain that frequencies detuning $p \neq 0$ leads only to a change of form-factor ($\mathrm{Re}(\delta q) \neq 0$, $\mathrm{Im}(\delta q) = 0$). Using (9), (10) we may calculate the response functions K_S^m for $N = 2$, $m = 1, 2$

$$K_S^1 = \frac{3}{2}\mathrm{sech}^3(\tau),$$

$$K_S^2 = 2\mathrm{sech}(\tau)\left[1 - \frac{3}{4}\mathrm{sech}^2(\tau)\right],$$

$$K_A^1 = -\frac{3}{2}\mathrm{sh}(\tau)\mathrm{sech}^4(\tau),$$

$$K_A^2 = \mathrm{sh}(\tau)\mathrm{sech}^2(\tau)\left[\frac{9}{2}\mathrm{sech}^2(\tau) - 2\right]. \quad (12)$$

Substituting (6) and (12) into (8), we obtain, after integration, the expression for the form-factor perturbance for the both solitons

$$\delta\kappa_1 = -p^2 f(p),\ \delta\kappa_2 = -4[1 - f(p)] - p^2 f(p) \quad (13)$$

where $f(p) = (\pi p/2)/\mathrm{sh}(\pi p/2)$. As $p \to 0$, the perturbances of the form-factors have the asymptotics $\delta\kappa_1 = -p^2$, $\delta\kappa_2 = -(\pi^2/6 + 1)p^2$.

The dependencies of $\kappa_1 = 3 + \delta\kappa_1$ and $\kappa_2 = 1 + \delta\kappa_2$ on p corresponding to (13) are shown on Fig. 1(a). One can see that as p increases, form-factors of both solitons decrease and at $p \approx 0.5$ 2-solitons bound state transforms into one-soliton pulse with the form-factor $\kappa_1 \approx 2.75$. From our point of view, it is a practically interesting result, because for an input signal one can obtain a one-soliton pulse with approximately three times less duration.

Numerical analysis When the parameter of frequency detuning p increases ($p > 0.5$), the conditions of using of the perturbance method of inverse scattering transform are not valid, because δq is not small. In such a case, it is necessary to use the numerical IST-based method for calculation of eigenvalues Λ_m of (4). The key elements of this method are discussed in [7], so we shall restrict the discussion to the main results.

In Fig. 1(a) the dependencies of form-factors κ_1, κ_2 on p are shown. As it is seen from Fig. 1(a), for $p < 0.5$, these dependencies are in good agreement with the analytical result (13). For $p \approx 1.51$, the character of the solution essentially changes: from initial condition (3) two separating solitons are forming with the same form-factors but with opposite (in sign) velocities. These solitons are going in opposte directions with respect to each other, while propagating along the fiber. The dependence of velocity V_2 on p is shown on Fig. 1(b) ($V_1(p) = -V_2(p)$). We see that $|V_{1,2}| \to p$ when $p \to \infty$, and difference $|V_2 - p|$ is proportional to p^{-2} in agreement with the analytical result [2]. Also we note that the value of p, when two separated solitons appear, approximately

corresponds to value of p at which Hamiltonian of (1) $H(p) = 0$.

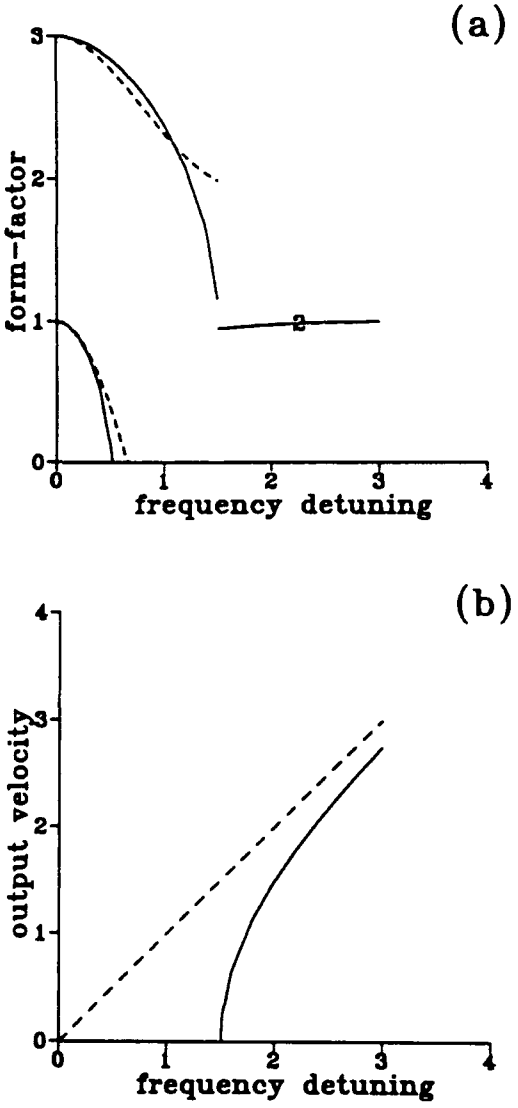

Fig. 1. The form-factors $\kappa_{1,2}$ (a) and velocity V_2 (b) of 2-soliton initial condition pulse (5) as a function of p. In Fig.1(a) the dashed lines were calculated by the analytical approach (13), the solid lines — numerical calculations of eigenvalues (4). The line marked (-2-) corresponds to two separating solitons with the same form-factors and opposite velocities. In Fig.1(b) the solid line — result of calculations, dashed line is the limit of $V = p$.

For modelling the dynamics of the transitional process we use the direct numerical methods for solving NLS equation (1). In Fig. 2 is shown the pulse shape transformation along the fiber. The case in Fig. 2(a) illustrates the dynamics of forming of the one-soliton pulse, and Fig. 2(b) - the dynamics of two separated solitons. The soliton parameters, calculated by the direct numerical solution (1) for $z > 1$, and by the method of inverse scattering transform are in a good agreement.

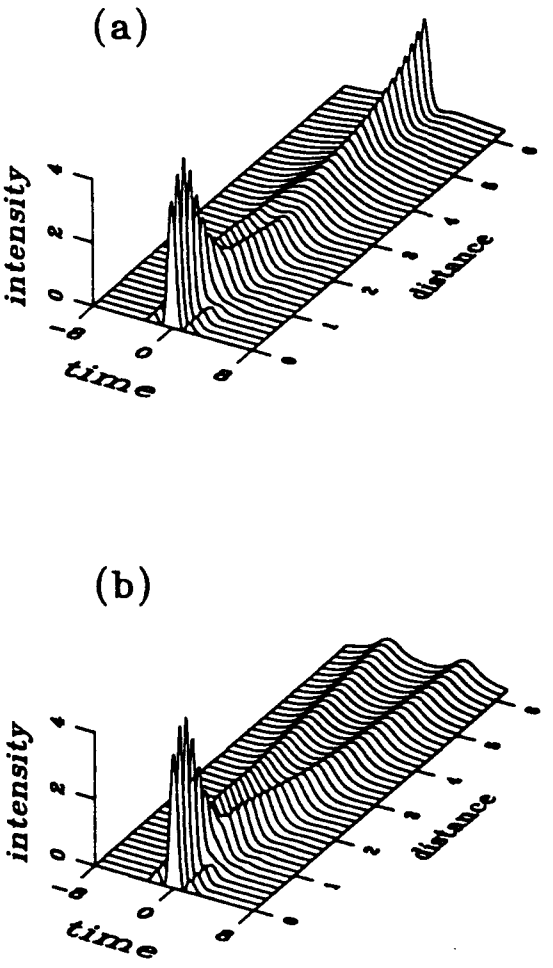

Fig. 2. Transformation of the pulse shape along the fiber at $p = 1.45$ (a) and $p = 1.55$ (b). In case (a) the one-soliton pulse is forming with $\kappa_1 \approx 1.37$ and $V_1 = 0$ and in case (b) two solitons are forming with $\kappa_{1,2} \approx 0.95$ and velocities $V_2 = -V_1 \approx 0.36$.

The results presented above address the case of the same phases ($\phi = 0$) and same initial coordinates ($\tau_s = 0$) of the solitons. In Fig. 3 are shown the calculated dependencies of form-factors κ_1 and κ_2 on the time delay for fixing frequency mismatch $p = 0.5$.

One can see that as τ_s increases, $\kappa_1 \rightarrow \kappa_2 \rightarrow 1$. This limit case ($\tau_s \rightarrow 1$) corresponds the problem of the collision of Schrödinger solitons, moving with different velocities. It is known [3] that after a collision the form-factors and velocities remain unchanged. Figs. 3(b) illustrates the dependencies of κ_1 κ_2 on the initial phase mismatch ϕ for two values of p.

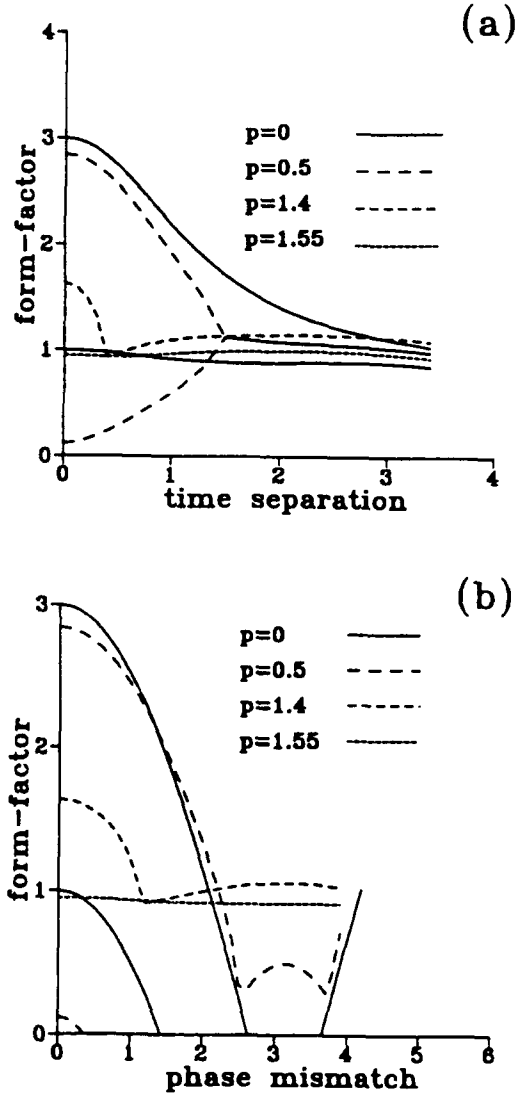

Fig. 3. The form-factors of 2-soliton pulse (5) as a function of time delay τ_s (a) and as a function of phase mismatch ϕ for various values of frequency detuning p.

Conclusion Note that the technique of nonlinear soliton mixing in optical fibers with different wavelength give the new possibilities for controlling the soliton parameters. These possibilities expand significantly when we pass from 2- to N-soliton pulses. For example, Fig.4 illustrates the 3-soliton cases. The dependencies of $\kappa_m(p)$ are shown for initial pulse (5) at $N = 3$ (dashed lines). Additionally we calculated $\kappa_m(p)$ for initial conditions $q_0(\tau) = [1 + 2\cos(p\tau)]\mathrm{sech}(\tau)$ (Fig.4, solid lines). This initial condition corresponds to 3-channel spectral multiplexing. In particular, mixing of three solitons with different carrying frequencies at $p = 1.4$ results in forming of the one-soliton pulse with $\kappa \approx 4.5$.

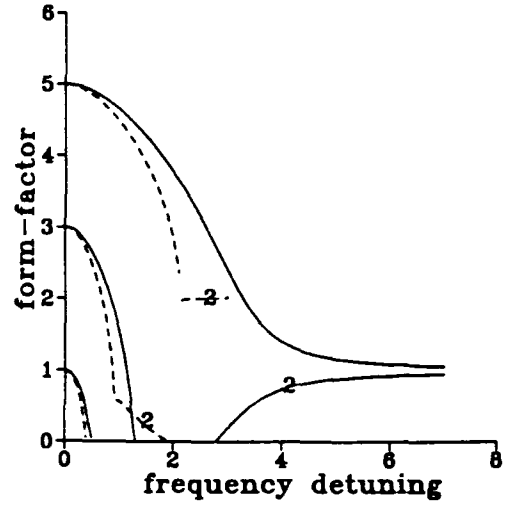

Fig. 4. The form-factors κ_m of 3-soliton initial conditions $q_0(\tau) = 3\cos(p\tau)\mathrm{sech}(\tau)$ (dashed lines) and $q_0(\tau) = [1 + 2\cos(p\tau)]\mathrm{sech}(\tau)$ (solid lines) as a function of frequency detuning p. The lines marked (-2-) correspond to two separating solitons with the same form-factors and opposite velocities.

References

1. A. Hasegawa, Optical Solitons in Fibers, Springer-Verlag, Berlin (1989).

2. Y. Kodama and A. Hasegawa, Opt. Lett. **16**, 208-210 (1991).

3. V.E. Zakharov and A.B. Shabat, Sov. Phys. JETP,**34**, 62-69 (1972).

4. P.A. Andrekson, V.A. Olsson, J.R. Simpson, T. Tanbun-Ek, R.A. Logan, P.C. Becker, and K.W. Wecht, Appl. Phys. Lett. **57**, 1715-1719 (1990).

5. J. Satsuma and N. Yajima, Progr. Theor. Phys., Suppl. **55**, 284-306 (1974).

6. V.A. Vysloukh, A.V. Ivanov, I.V. Cherednik, *Ultrafast Phenomena in Spectroscopy* - Proc. 5-th Int. Symp., (August 22-25, 1987, Vilnius, USSR) - Singapore: World Sc. Publ. 1988, p. 179-186; V.A. Vysloukh, I.V. Ivanov, I.V. Cherednik, Izv. AN SSSR, ser. fiz., **53**, 1514-1519 (1989).

7. S.A. Akhmanov, V.A. Vysloukh, and A.S. Chirkin, Optics of femtosecond laser pulses, Moscow, Nauka, 1988 (in Russian, will be translated in English in Springer-Verlag, 1991).

Nonlinear Directional Coupler in $Al_{0.18}Ga_{0.82}As$ Near Half the Band Gap.

J. S. Aitchison, A. H. Kean and C. N. Ironside,
Department of Electronics and Electrical Engineering,
University of Glasgow,
Glasgow, G12 8QQ

A. Villeneuve and G. I. Stegeman,
CREOL,
University of Central Florida,
Orlando, FL, 32826

Abstract:

We report the first experimental observation of an ultrafast all-optical switch in a semiconductor waveguide configuration where the transmission is not limited by absorption processes.

Introduction

There has been considerable interest in all-optical switching devices which utilise the nonresonant contribution to the nonlinear refractive index, n_2. The nonresonant nature of the effect makes the response time of such devices in the femtosecond region. To date nonresonant effects have been confined to glass waveguides and fibres, where the low absorption available has allowed the high optical intensities required to propagate without causing damage to the sample.

Semiconductors could potentially be much more efficient devices, recent theoretical investigations predict relatively large values of n_2 close to half the fundamental band gap[1]. The predicted value of n_2, the nonresonant contribution to the nonlinear refractive index, is plotted in figure 1. Previous investigations into all-optical switching in semiconductor waveguides have been limited by the two-photon absorption effect[2,3]. Indeed the photo-excited carriers generated by the two-photon process induce a negative index change which washes out the smaller, positive contribution from the nonresonant term, the two-photon band edge is also plotted in fig 1.

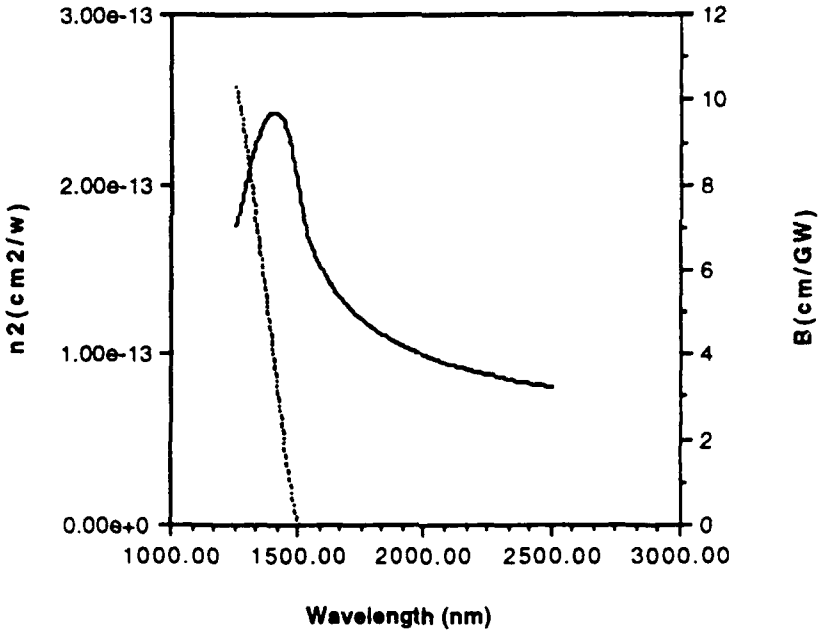

Fig. 1 Theoretical plot of n_2 showing the resonance close to the two-photon absorption edge and β, the two-photon absorption coefficient, as a function of wavelength, nearhalf the fundamental band-gap.

We present the first experimental demonstration of an all-optical switch, in a semiconductor waveguide, where the transmission of the device is not limited by two-photon absorption. The AlGaAs waveguides contained sufficient Al to shift the band edge towards the visible, so that TPA would not be a problem in the 1.55 μm spectral region. Initial experiments performed on a similar waveguide structure have shown spectral broadening close to the two-photon band-edge[4].

The waveguides used in this investigation were fabricated from an MBE grown wafer with the following layer structure. The substrate was n^+ GaAs, on which a 4 μm thick

isolation layer of $Al_{0.25}Ga_{0.75}As$ was grown. The relatively thick isolation layer was used to reduce losses due to the high index GaAs substrate. The high index waveguiding layer consisted of a 1.5 μm thick layer of $Al_{0.18}Ga_{0.82}As$ and finally the cladding consisted of a 1.5 μm layer of $Al_{0.25}Ga_{0.75}As$. All layers were un-doped. Directional couplers were fabricated by a combination of photolithography and reactive ion etching, to depths of 1.2-1.45 μm. To ensure that all of the input power was coupled into a single arm of the directional coupler, the devices were fabricated with a single input channel, the second guide starting ~1mm from the input facet.

The TE_0 mode was excited by endfire coupling the output from a synchronously pumped, mode-locked NaCl:OH^- colour centre laser, into the input arm of the directional coupler using a 20X microscope objective. The laser produced 10ps pulses which were tuneable across the low-loss telecommunications window around 1.55 μm. The output of the coupler was collected using a 60X microscope objective, allowing the light from the two output channels to be spatially separated onto two Ge photodetectors. The input intensity was controlled using a computer driven half-waveplate/polariser combination. The output from both the bar and cross states, together with the input power were recorded by chopping the beam and connecting the detectors to the computer via lockin amplifiers.

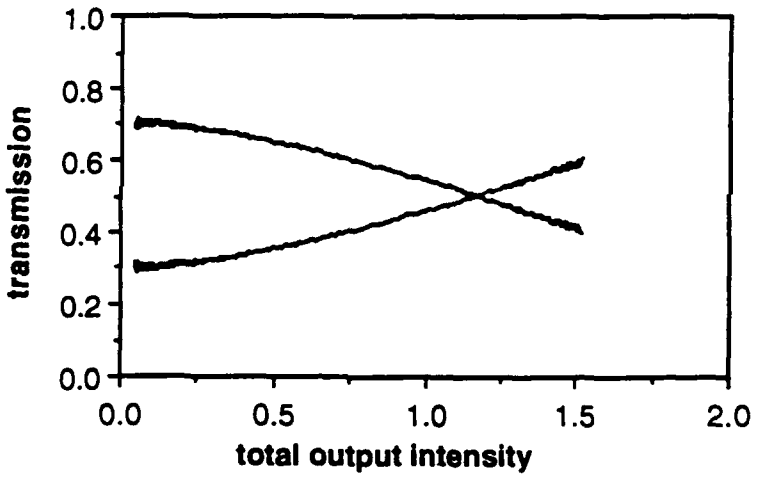

Fig 2. Transmission of the bar and cross states for the nonlinear coupler as a function of total output intensity. The data was taken at λ=1.56 μm.

Figure 2 shows a plot of the experimentally measured transmission of the bar and cross stated of a directional coupler with a 6.25 mm long coupling section, as a function of the total output power. The coupler consisted of 4 μm wide waveguides separated by 5μm, the input wavelength was 1.56 μm. From figure 2 it is clear that the transmission of the bar and cross states has become a function of intensity and switching between the two states can clearly be seen.

The coupling length of the device was determined by a) a theoretical model using the known properties of the device and b) comparison of all couplers with the same waveguide width on the chip to the predicted results of the model. Using this model we were able to predict that the coupler used in these experiments had a coupling length of $0.63L_c$ at 1.56 μm. The switching of the device was limited by the total power available from the colour centre laser.

The switching response of the nonlinear directional coupler has been predicted by Jensen[5], using coupled mode theory. The CW response of the nonlinear coupler is given by:

$$I_b(L) = I(0)\left[1 + cn\left(\frac{\pi L}{L_c} | m\right)\right] / 2 \qquad \text{equ. 1}$$

Where L is the length of the coupling section, L_C is the coupling length, $m=[I(0)/I_C]^2$, $I_b(L)$ is the output intensity of the bar state, I(O) is the input intensity, cn(ulm) is a Jacobi elliptic function and I_C is given by:

$$I_c = \frac{\lambda}{L_c n_2}$$

For a nonlinear coupler with a responce time which is much faster than that of the detection system used we need to examine the time average of equ. 1, this is plotted in figure 3 for a nonlinear coupler of length $L=0.63\ L_C$ as can be seen by comparing figures 2 and 3 the nonlinear coupler is behaving as predicted by coupled mode theory.

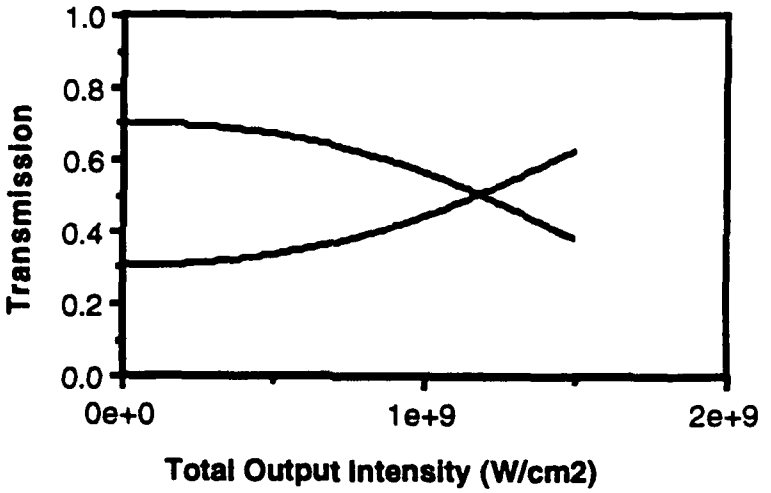

Fig 3.Theoretical plot of transmission against total output intensity for a coupler of length $L= 0.63L_C$.

By comparing figures 2 and 3 we were able to determine the magnitude of n2 for $Al_{0.18}Ga_{0.82}As$, at 1.56 μm, to be 9.5×10^{-14} cm^2 W^{-1}.

To determine the underlying mechanism giving rise to the effect, we performed a pump-probe experiment on the nonlinear coupler: A low power probe pulse was split off from the main input beam, delayed by 50 ps, and coupled into the waveguide. The transmission of the delayed probe was measured as a function of pump power. No evidence of switching was observed by the delayed probe pulse. If the underlying mechanism was thermal in nature then the response time would be around a microsecond or if it was due to photo-generated carriers then the recovery would be of the order of a few nanoseconds.

In conclusion we have demonstrated switching in an $Al_{0.18}Ga_{0.82}As$ directional coupler in the 1.55 μm spectral region. Pump-probe experiments have eliminated the possibility that the underlying mechanism is thermal or due to photo-generated carriers. Our

experimentally determined value of $n_2=9.5 \times 10^{-14}$ cm^2W^{-1}, which is consistent with that predicted by theory.

References:

1. M. Sheik-Bahae, D.C. Hutchings, D.J. Hagan and E.W. Van Stryland, IEEE J **QE-27**, pp. 1296-1309, (1991)

2. J.S. Aitchison, M.K. Oliver, E.Kapon, E. Colas, and P.W.E. Smith, Appl. Phys. Lett.'**56**, pp.1305-1307, 1990

3. A. Villeneuve, M. Sundheimer, N. Finlayson, G.I.Stegeman, S. Morasca, C. Rigo, R. Calvani and C. De Bernardi. Appl. Phys. Lett. 56, pp. 1865-1867, (1990)

4. S.T. Ho, C.E. Soccolich, W.S. Hobson, A.F. Levi, M.N. Islam and R.E. Slusher Postdeadline paper at IQEC'91, Baltimore, 1991

5. S.M. Jensen, IEEE J **QE-18**, pp. 1580-1583, (1982)

Nonlinearity Near Half-Gap in Bulk and Quantum Well GaAs/AlGaAs Waveguides

M.N. Islam,[a)] C.E. Soccolich,[a)] R.E. Slusher,[b)] A. F. J. Levi,[b)] W. S. Hobson,[b)] and M.G. Young [a)]
a) AT&T Bell Laboratories, Holmdel, NJ 07733
b) AT&T Bell Laboratories, Murray Hill, NJ 07974

We present measurements of the nonlinear index n_2 and two-photon absorption coefficient β as well as time resolved pump-probe data for both bulk AlGaAs and GaAs/AlGaAs multiple quantum well waveguides near half-gap at 1.68 μm. The figure of merit ($2n_2/\beta\lambda$) [1] for the bulk (MQW) material is 17 (1.6), which means that these semiconductors below half bandgap are appropriate for all-optical switching and quantum optics applications. The β value is up to 25 times larger in the MQW. This larger value may result from mid-gap states that act as a stepping stone in two-photon absorption (TPA). The mid-gap absorption should not be fundamental to MQW material provided that caution is exercised during the growth to avoid impurities and interface states. We confirm that n_2 is instantaneous on the 300 fs time scale of our pulses from self-phase-modulation spectra as well as time-resolved pump-probe measurements. However, we find an intriguing exchange of energy between the two orthogonal axes with the signal along the probe axis following the negative derivative of the pump. This result may be explained by self-phase-modulation of the pump combined with a low frequency Raman gain between orthogonal axes.

Our laser source is a passively modelocked NaCl color center laser whose output is separated into orthogonally polarized pump and probe beams. A stepper-motor controlled delay line is used to vary the time separation between the two pulses, which are recombined at a polarizing beam splitter and then sent to the waveguides. In the bulk samples a ridge waveguide is formed in a 2.55μm thick layer of $Al_{0.2}Ga_{0.8}As$, and guiding is provided by a 2.55μm underlying layer of $Al_{0.5}Ga_{0.5}As$. The ridge height is 0.7μm and its width is 4.5μm [2]. The MQW and bulk waveguides are grown in different MOCVD reactors that may, for example, have different levels of oxygen impurities. The MQW waveguide core consists of 200 periods of 40 Å GaAs wells and 70 Å $Al_{0.3}Ga_{0.7}As$ barriers. We assure guiding in the vertical dimension by using a 3 μm thick layer of lower index $Al_{0.3}Ga_{0.7}As$ below the MQW guide, and lateral confinement is provided by etching a 2 μm wide ridge with a 0.6μm height.

As in the case for optical fibers, we can use the simple self-phase-modulation spectral technique for measuring n_2 in our semiconductor waveguides. In the bulk material the intensity required for a π phase shift is 3.1±0.5 GW/cm^2, which yields a value of n_2=+3.6(±0.5)×10^{-14}cm^2/W. In the MQW for the electric field polarized in the plane of the quantum wells $\hat{e}\perp\hat{z}$ we obtain $n_2 = +8.7(\pm1.7)\times10^{-14}cm^2/W$, and for the polarization perpendicular to the quantum wells $\hat{e}\|\hat{z}$ we find a value of $n_2 = +5.4(\pm1)\times10^{-14}cm^2/W$. We attribute the up to 2.4 times enhancement in the MQW to a stronger 1S-exciton intermediate state. The maximum enhancement in the quantum wells should be proportional to the ratio of three-dimensional to quasi-two-dimensional exciton volume multiplied by a filling factor to account for the fraction of material in the wells. For the parameters in our MQW we calculate a theoretical maximum enhancement of ≈3.4 that is peaked close to the TPA band edge. We expect to observe less than the maximum enhancement since: (1) we are ~ 60 meV away from the onset of TPA; and (2) the observed nonlinearity results not only from the 1S-exciton intermediate state, but also through other states that are not as strongly confined. Therefore, our measured enhancement of 2.4 (1.5) for $\hat{e}\perp\hat{z}$ ($\hat{e}\|\hat{z}$) is reasonable.

To measure β in the MQW material we measure the transmission of a single beam as a function of input intensity. Following the procedure in Ref. [1], we plot the reciprocal of the transmission versus input power and, after correcting for the Gaussian pulse profile, extract β from the slope. For $\hat{e}\perp\hat{z}$ we obtain an average value of $\beta = 6.5\pm1\times10^{-4}$ cm/MW, and for $\hat{e}\|\hat{z}$ we obtain a lower average value of $\beta = 4\pm0.6\times10^{-4}$ cm / MW. The nonlinear absorption is much weaker in our bulk material; so, for a more accurate measure including three-photon absorption, we study the nonlinear loss using a probe beam [2]. By fitting the probe absorption coefficient we obtain $\beta = 0.26\times10^{-4}$cm/MW and a three-photon absorption coefficient of $\alpha_3 = 0.004cm^3/GW^2$.

The larger values for β in the MQW samples should not be fundamental to MQW material and probably arise because of mid-gap or deep level states in the material. The larger concentration of mid-gap states in the MQW may be due to interface states, higher levels of impurities, or differences in the MOCVD reactors in which the two samples were grown. Further evidence that suggests the existence of mid-gap states in our MQW material is found from pump-probe measurements. For the probe preceding the pump ($\delta t<0$) we find a pronounced difference between the bulk and MQW material. Whereas in the bulk the transmission of the probe does not change with and without the pump, for the MQW there is a decrease in the probe transmission when the pump is added even for $\delta t<0$. To understand the origin of this long-lived background in the MQW material, we studied the change in transmission of the probe (with and without the pump) for $\delta t<0$ as a function of pump power. In Fig. 1 we plot $\alpha L = -\ln[1-\Delta T/T_o]$, which is the total pump induced absorption coefficient, versus the average pump intensity at the waveguide input. The slope of the absorption at low pump intensity indicates a $\chi^{(3)}$ process and the long time constant (> 12 ns) is consistent with mid-gap state mediated TPA. In bulk material mid-gap states may have lifetimes of between 1-10ns. On the other hand, in MQW if the electrons escape from the wells and become spatially separated from the ionized centers, then the lifetimes may extend into the microsecond range.

We also perform time-resolved pump-probe measurements with orthogonally polarized pump and probe pulses. Only the probe beam is modulated, and the signal from the detector at the waveguide output is fed to a lock-in that is referenced to the same modulation frequency. Other than the background for $\delta t<0$ in the MQW, we observe the same kind of temporal behavior in the bulk and MQW. Therefore, to avoid complications from the long-lived background, we show here the pump-probe data as a function of pump power for the bulk sample. In Fig. 2 we include three sets of data that are collected as a function of pump power: (a) no polarizer to see the complete change in output due both to the pump and probe; (b) polarizer at output along probe axis to see the change in probe due to the pump beam; and (c) polarizer at output along pump axis to see the change in pump due to the probe. Note that although the three curves of each set in Fig. 2 are drawn on the same scale, the various data are displaced for ease of display. With no polarizer at the waveguide output we observe the expected behavior for multi-photon absorption. For example, in Fig. 3 we plot the normalized peak change in transmission ($\Delta T/T$) as a function of peak pump

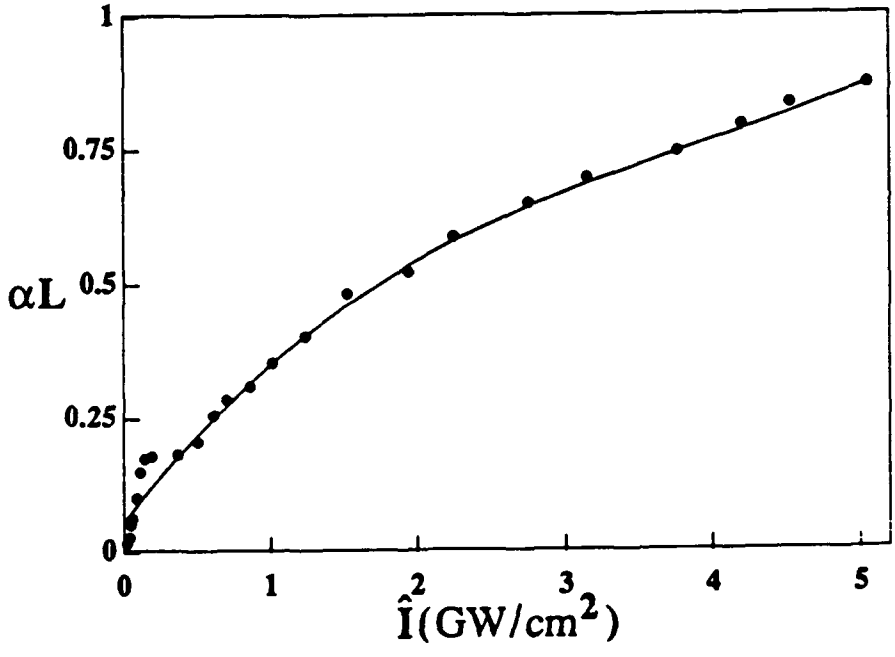

Fig. 1 Change in transmission of the probe with and without the pump ($\alpha L = -\ln[1-\Delta T/T_o]$) for $\delta t<0$ as a function of average pump intensity in the MQW waveguides.

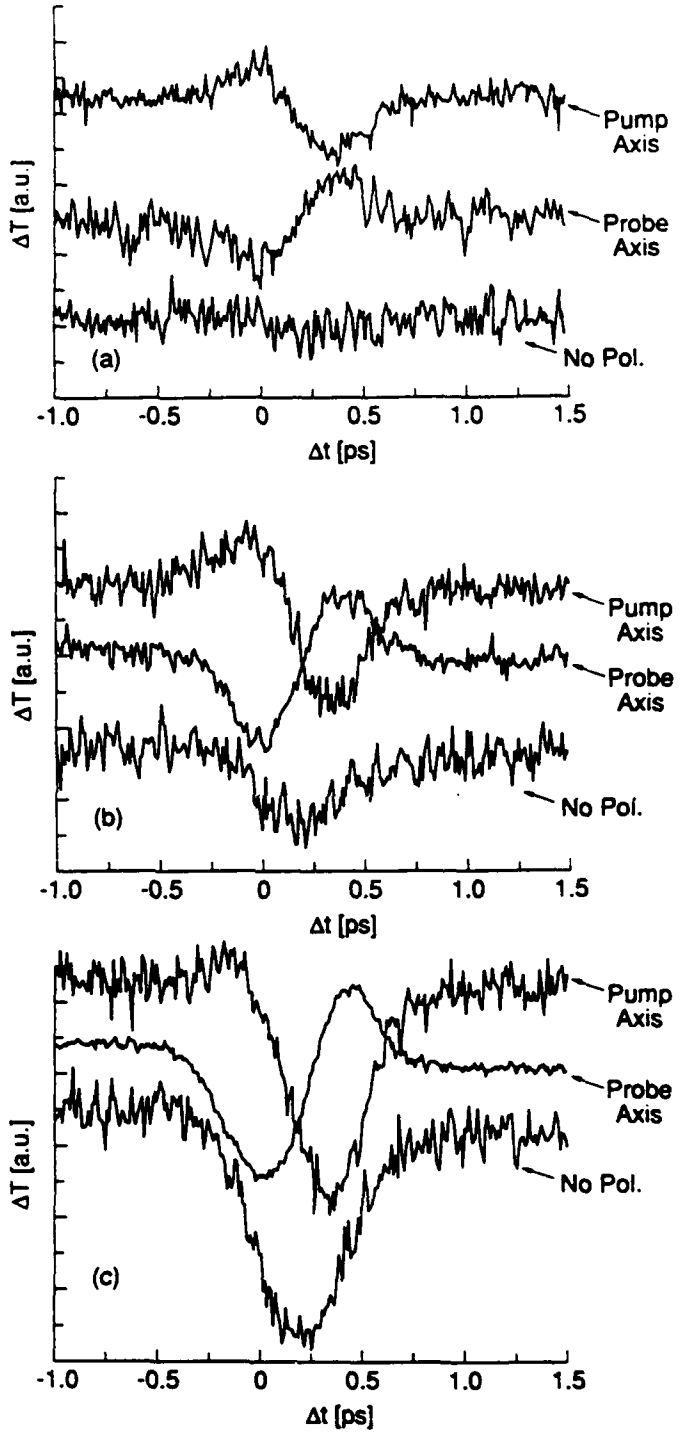

Fig. 2 Time-resolved pump-probe data using 285 fs pulses at 1.67μm with no polarizer, polarizer at output along probe axis, and polarizer at output along pump axis. The pump intensity at the output of the bulk waveguide corresponds to: (a) 0.38; (b) 1.34; and (c)3.85 GW/cm^2.

intensity at the bulk waveguide input and find contributions from two and three photon absorption. When we add the polarizer to the waveguide output, the behavior becomes much more complicated in both the bulk and MQW. The probe pulse is attenuated when overlapped with the leading edge of the pump pulse and amplified in the trailing edge. In Fig. 3 we also include the peak-to-peak change $\Delta T/T$ of the probe and see a linear behavior, thus confirming that the derivative-like signal is due to a $\chi^{(3)}$ process . Note that when the probe rises above its level for $\delta t<0$ that the probe experiences significant gain (as large as 15%), indicating a transfer of energy between the two axes.

One possible explanation for the exchange of energy between the two axes is a low frequency Raman gain. Self-phase-modulation chirps the pump pulse (red-shifts the leading edge and blue-shifts the trailing edge), while Raman gain transfers energy from the higher to the lower frequency pulse. The data implies a Raman coefficient between orthogonally polarized pulses of $R_\perp \sim 5.5\times10^{-11}$cm/W for $\Delta\nu\lesssim30\text{cm}^{-1}$, which is more than two orders of magnitude larger than in fused silica fibers for comparable $\Delta\nu$. A low frequency Raman gain of this magnitude may arise in the AlGaAs alloy, where the random occupation of sites relaxes the k-conservation rule for first order Raman scattering. In addition, even in the perfect crystal there are second order Brillouin processes that involve two phonons and that are Raman-like; i.e. wave vector conservation is satisfied by the difference between two acoustic phonon wave vectors.

In summary, we have measured the real and imaginary components of $\chi^{(3)}$ near the half-gap in bulk AlGaAs and GaAs/AlGaAs MQW waveguides. For the bulk material we find $n_2=+3.6\times10^{-14}\text{cm}^2$ /W and $\beta=0.26\times10^{-4}$cm/MW, which imply a figure of merit $F_m=17$. In the MQW we find that the nonlinearity is enhanced up to 2.4 times over the value in bulk, which is consistent with the maximum enhancement expected from the 1S intermediate state. Finally, time-resolved pump-probe measurements confirm that the nonlinearity is instantaneous and show that at least two mechanisms are responsible for the derivative-like behavior along the probe axis.

[1] V. Mizrahi, K.W. DeLong, G.I. Stegeman, M.A. Saifi and M.J. Andrejco, Opt. Lett. 14 , 1140 (1989).

[2] S.T. Ho, C.E. Soccolich, W.S. Hobson, A.F.J. Levi, M.N. Islam and R.E. Slusher, "Large Nonlinear Phase Shifts in Low-Loss AlGaAs Waveguides Near Half-Gap," (to be published in Appl. Phys. Lett.).

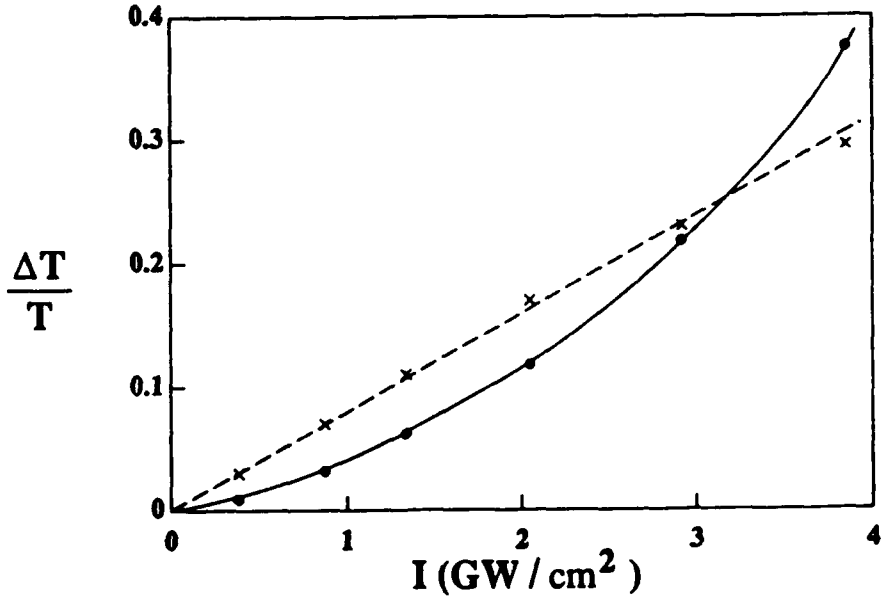

Fig. 3 Peak-to-peak change in transmission $\Delta T/T$ normalized to the probe transmission in the bulk waveguide as a function of output pump intensity. The solid dots correspond to no polarizer, and the ×'s correspond to a polarizer at the output along the probe axis.

Field Dependent All-optical Switching in GaAs/AlGaAs Quantum Well Waveguide operating beyond the Two Photon Absorption Limit

H.K.Tsang, R.V.Penty and I.H.White

University of Bath, School of Physics, Bath BA2 7AY, U.K.
(Telephone +225-826826 ext. 5155, Telefax +225-826110)

R.S.Grant, W.Sibbett

University of St.Andrews, Dept. of Physics and Astronomy,
St. Andrews KY16 9SS, U.K.

J.B.D.Soole, E.Colas, N.C.Andreadakis, H.P.LeBlanc

Bellcore, 331 Newman Springs Road, Red Bank NJ07701, USA.

Recently, two photon absorption (TPA) in semiconductor materials has been found to impose a serious limitation on the amount of ultrafast optically induced phase modulation available for use in all-optical switching elements[1]. The limit arises because nonlinear absorption reduces the effective available nonlinear length of an element so that it is not possible to obtain large, ultrafast, all-optical phase modulation at a given switching power by merely increasing the device length. To date the magnitude of ultrafast all-optical phase modulation in semiconductor materials operating relatively close to the bandgap has proved insufficient for their use in all all-optical switching structures[2,3], although it has been possible to obtain sufficient phase modulation by using the relatively slow (>50ps recovery time) refractive index change from photogenerated carriers[4]. In this paper we demonstrate that it is possible to work beyond the TPA limit by operating close to the half bandgap wavelength where TPA is minimal. We have observed over π radians ultrafast all-optical phase modulation in a GaAs/AlGaAs multi-quantum well (MQW) waveguide and have characterised the field and polarization dependences of the nonlinear absorption near half bandgap. These measurements show that GaAs/AlGaAs MQW waveguides can be successfully used for ultrafast all-optical switching in the 1.55μm optical fiber communications band.

The GaAs/AlGaAs MQW waveguides used in the measurements had an n doped MQW region ($n\sim10^{17}$ cm^{-3}) formed by 54 GaAs quantum wells of 5nm nominal width and 53 4nm wide $Al_{0.45}Ga_{0.55}As$ barriers. The MQW region was grown on top of a n-doped $Al_{0.45}Ga_{0.55}As$ buffer layer deposited on a [001] orientated n+ GaAs substrate. A 1μm thick p-doped $Al_{0.45}Ga_{0.55}As$ ($p\sim5x10^{16}$ cm^{-3}) was grown on the MQW region and this acted as the top cladding layer of the waveguide. Ribs of 0.55μm height and 4μm width running in the $[1\bar{1}0]$ crystal direction were etched in the top cladding layer. Ohmic metal contact was made to the top and bottom of the waveguides to allow an electric field to be applied across the MQW. The waveguides used in the experiment were cleaved to 3mm length and anti-reflection coated for the 1.5-1.6μm band. Room temperature photoluminesence measurements of the MQW material indicated that the 'bandgap' (electron-heavy hole transition) of the quantum wells corresponded to a wavelength of 814nm.

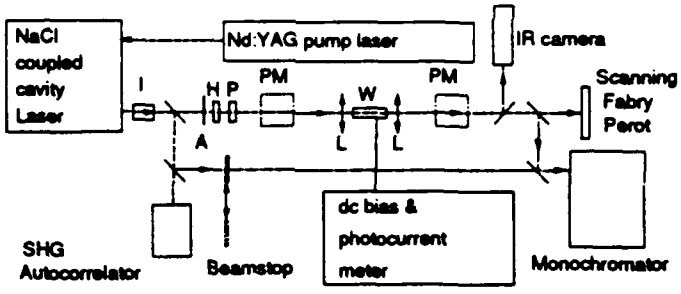

Figure 1 Experimental set-up to measure nonlinear absorption and self phase modulation. I=optical isolator, H=halfwave plate, P=polarizer, A=attenuator wheel, PM=power meter (inserted when required), L=lens, W=MQW waveguide.

Figure 1 shows the experimental set-up. A coupled cavity mode-locked NaCl color center laser provided pulses of typically 250fs duration at a repetition rate of 164MHz. The pulses were tuneable in the 1.55-1.63μm spectral region using a single birefringent plate. The light was coupled into the MQW waveguide using a 0.5NA lens. The polarization of the incident optical pulses was set to either TE or TM by means of a halfwave plate and polarizer, and the incident optical power was varied using an attenuator wheel. The nonlinear absorption for each polarization was characterized by measuring the waveguide transmission and photocurrent at different incident powers and electrical biases. By measuring the optical spectra of the transmitted pulses, it was possible to determine the spectral broadening from self-phase modulation(SPM). Comparison of the spectral broadening due to SPM in the MQW waveguides with that due to SPM in a well characterised, monomode, dispersion-shifted optical fiber gave a measure of the of the nonlinear refraction in the MQW waveguide.

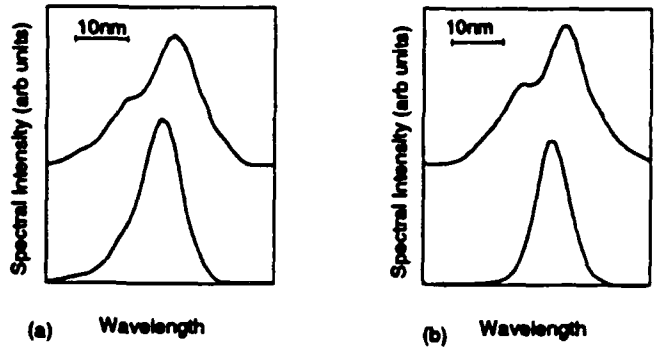

Figure 2(a) Output spectra at high (185W) peak input power and low (~10W) peak input power of 1.55μm TM light. (b) Spectra of 1.55μm pulses transmitted through 2.63m length of optical fiber at 530W peak input power (upper trace) andspectrum of the input pulse (lower trace).

Nonlinear refraction in the MQW waveguides gave rise to self-phase modulation (SPM) of the 250fs optical pulses. The spectral broadening from SPM (Figure 2) appeared on both sides of the spectral peak, indicating that the nonlinearity had rise and recovery times much shorter than the 250fs pulse duration[5]. The asymmetry of the spectra in Figure 2 was due to asymmetry present in the input pulses and also appeared when the pulses were passed through an optical fiber in a reference experiment (Fig. 2b). No significant polarization dependence in the spectral broadening was observed in the output from the MQW waveguides.

By comparing the spectral broadening due to SPM in the MQW waveguides (Fig. 2a) with that due to SPM in a well characterised optical fiber (Fig. 2b), an estimate of the nonlinearity in the MQW waveguide was possible. The spectral broadening shown in Fig. 2 corresponded to ~4 radians phase change, implying a value for the nonlinear refractive index coefficient n_2 of ~$9 \times 10^{-14} cm^2/W$.

In the experiment, the average photocurrent was found to be proportional to the square of the input power, for input powers up to 200W peak, the maximum used in the measurements. Thus for the power levels employed, two photon absorption dominated over three-photon or higher order absorption. The value of the TPA coefficient at a particular wavelength was determined by employing the usual technique of plotting 1/transmission versus the input power (Figure 3a). Plots similar to Figure 3a were obtained for different wavelengths in the 1.55μm to 1.63μm range . The values of the TPA coefficients obtained from such plots are shown in Figure 3b. The TPA coefficient for TE light decreased from 1.1cm/GW at 1.55μm to 0.15cm/GW at 1.628μm wavelength. The TPA coefficient for the TM polarization did not vary significantly over this wavelength range, measuring about ~0.15cm/GW. The strong polarization dependence at 1.55μm may be explained by the different energies of the electron-heavy hole (e-hh) transition (at 814nm) and electron-light hole (e-lh) transition (around 770nm) in the quantum well. Selection rules 'allow' the e-hh transition only for the TE polarization. Therefore at 1.55μm, TPA of TE light is possible involving the 'allowed' e-hh transitions whereas TPA of TM light is only energetically possible by 'forbidden' e-hh transitions or transitions to band-tail states.

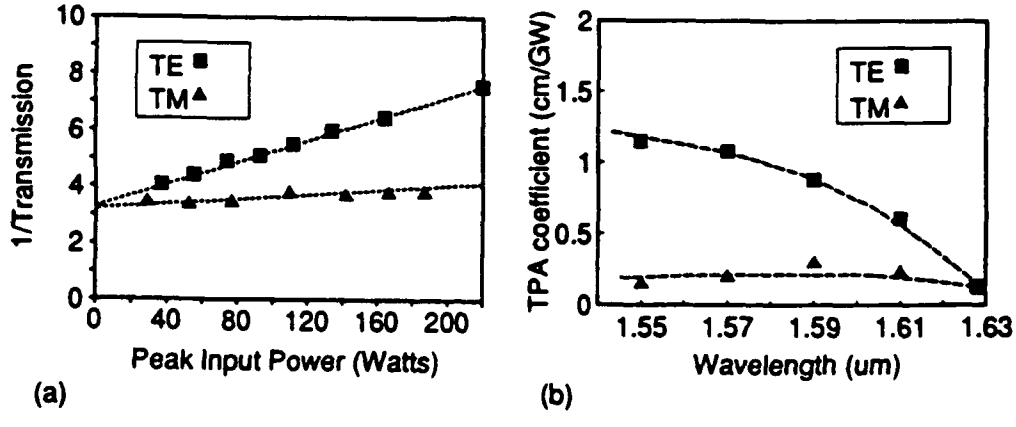

Figure 3(a) Typical plot from transmission measurements to give the TPA coefficient at a particular (1.55μm) wavelength. 3(b) Experimental values for the TPA coefficient for TE and TM light.

Application of an electric field produces a shift to lower energies of the e-hh and e-lh transitions as a result of the quantum confined Stark effect (QCSE). The wavelengths corresponding to the half bandgap energy will also be red shifted by the QCSE, thus increasing the TPA at wavelengths near the half bandgap. This was observed experimentally for both TE and TM light at wavelengths which corresponded to the half-energy of the e-hh and e-lh transitions respectively (Figure 3). At 1.55μm wavelength the TPA coefficient for TM light increased from 0.15cm/GW to 0.6cm/GW for a change in reverse bias from 0V to ~7.5-10V

(an electric field change of ~140kV/cm). For TE light at 1.55μm, the TPA coefficient did not exhibit any significant change with bias because of the large detuning from the e-hh half energy. At 1.63μm (at the e-hh half energy) the TPA coefficient for TE light increased from 0.1cm/GW to 0.6cm/GW for a change in reverse bias from 0V to ~7.5-10V. For TM light at 1.63μm there was no significant change in TPA with bias because of the large detuning from the e-lh transition. These observations are consistent with the QCSE.

A figure of merit[1], $T=\beta\lambda/n_2$, where β is the TPA coefficient, is often used to characterize the suitability of a material for all-optical switching. For the GaAs/AlGaAs MQW waveguides, the figure of merit takes a value of T=0.25 for TM light at 1.55μm, easily satisfying the criterion for an all-optical Mach Zehnder switch of T<2. This figure contrasts dramatically with the value at wavelengths closer to the single photon absorption edge[1], where T~20.

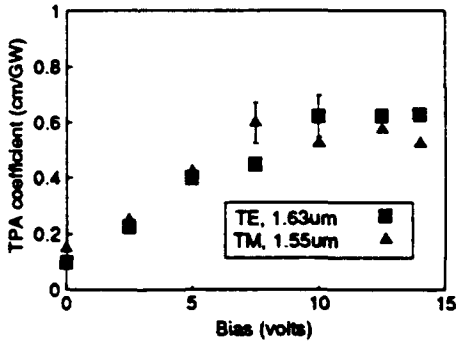

Figure 4 Experimental values of the TPA coefficient at different biases for TE light at 1.63μm and TM light at 1.55μm.

In summary, we have made the first observation of a field dependent TPA and observed large nonlinear refraction with relaxation times of <250fs. The refractive nonlinearity reported here for the GaAs/AlGaAs MQW waveguides is sufficiently large, and the TPA coefficient sufficiently small, to allow the implementation of an ultrafast all-optical switch. The GaAs/AlGaAs MQW material, operating near half-bandgap, is the best candidate for an ultrafast integrated semiconductor all-optical switch reported to date.

References

1. K.W.Delong and G.I.Stegeman, Appl. Phys. Lett. 57 2063 (1990).

2. A.Villeneuve, M.Sundheimer, N. Finlayson and G.I.Stegeman, Appl. Phys. Lett. 56 1865 (1990).

3. J.S.Aitchison, M.K.Oliver, E.Kapon, E.Colas and P.W.E.Smith, Appl. Phys. Lett. 56 1305 (1990).

4 R.V.Penty, H.K.Tsang, I.H.White, R.S.Grant, W.Sibbett and J.E.A. Whiteaway, Electron. Lett. 27 1447 (1991).

5. G.P.Agrawal, Nonlinear Fiber Optics (Academic Press), chapter 4 (1989).

6. W.L.Smith, CRC Handbook of Laser Science and Technology, (CRC Cleveland, Ohio; ed. M.G.Weber), 229-279, (1986).

SECOND HARMONIC GENERATION IN OPTICAL FIBRES - THE ROLE OF THE LONGITUDINAL FIELDS IN SYMMETRY BREAKING

Mark G Sceats and Simon B Poole

Optical Fibre Technology Centre
University of Sydney NSW 2046
Australia

ABSTRACT

Seeded SHG in fibres is quantitatively explained by the proposition that the longitudinal field of the pump mode is involved in the ionisation of Ge-Si wrong bonds through a 3-photon ionisation process invoving two pump photons and one seed photon. This interference produces a grating of defects which has the correct inversion asymmetry to produce SHG. Optical pumping of the trapped electrons in Ge(1) centres developes an electrostatic field which produces SHG by the EFISH mechanism.

INTRODUCTION

The initial observation of efficient SHG in fibres has led to considerable speculation concerning the underlaying mechanism[1-12]. It is generally accepted that there is no description which is quantiatively accurate, and the principal reason for this is that the mechanism of symmetry breaking required to explain the high conversion efficiencies has not been discovered. In this paper we develop a model which quantiatively explains the effect.

THE MODEL

a. Symmetry Breaking - production of defects via the longitudinal fields.

The only mechanism proposed hithertoo which has the correct symmetry breaking involves either the DC field arising from the third-order susceptibility [4] (which is too small to drive structural changes) or the involvement of (unobserved) idler modes [12]. In this model[13], we recognise that the inversion asymmetry is developed through the involvement of the longitudinal fields of the modes in the formation of defect centres in the fibre core. These fields[14] have an azimuthal (θ) dependence such that the defect density will be created asymmetrically across the core of the fibre.

The first step is the creation of charged defect centres in the fibre stabilised by stress relief[15]. This occurs by ionisation of Ge-Si wrong bonds to produce a positive GeE' centre and a trapped electron in a nearby Ge(1) or Ge(2) centre. The production of these defects has been verified[16]. This is a 3-photon ionisation process involving 2 pump photons and 1 seed photon[17]. It is this combination which produces a grating along the fibre which has the correct beat length for quasi-phase matching the SHG process[4], ie $\pi/(2\beta_p - \beta_s)$, where β denotes a propagation constant.

Previously[3], it was believed that the fields responsible for this process were the transverse fields, but this simply gives a distribution of defects which is symmetric with regard to the

polarisation axis, say x. What is required is the formation of a defect distribution which is asymmeric with repect to x - ie one which varies as cos θ . In this paper, we recognise that such a contribution will arise if the z-(ie longitudinal) component of the pump field is involved in the ionisation process. This field is generally disregarded because the power in it is small relative to the transverse fields. However, it arises in optical fibres because of the confinement induced by the core-cladding interface[14], and the field strength becomes large in high Δ fibres of the type used to produce SHG. It is of order $(2\Delta)^{1/2}$ U/V, where U is the dimensionless eigenvalue of the pump field with a dimensionless size parameter V. This is about 13 % of the transverse field strength, and this is a considerable contribution in an interference process. For the HE_{11} mode the azimuthal dependence of the longitudinal field is cos θ , which has the correct asymmetry. Thus the longitudinal field, when involved in a three photon ionisation process through terms such as $E_{p,z}\ E_{p,x}\ E_{s,x}$, gives a grating of defects which breaks the inversion symmetry. The product of the radial and azimuthal field functions of these components defines the distribution function of GeE' defects in the core of the fibre.

b. Formation of electrostatic fields by optical pumping.

There is no macroscopic electrostatic field produced by the formation of these defects. This is because the asymmetric distribution functions of the positive GeE' centres and the negative Ge(1) and Ge(2) centres overlap. We note in passing that these centres do not recombine because the large nuclear displacement arising from the ionisation of the Ge-Si wrong bond irreversibly relieves the thermoelastic stress in the core of the fibre[15]. In a forthcoming paper[15], the authors will demonstrate that the mechanism of stress relief is the general basis behind the writing of permanent phase gratings in the cores of optical fibres by intense visible or uv-light.

We propose that an electrostatic field is produced in the core of the optical fibre by optical pumping. Firstly, we note that Ge(1) traps can be detrapped by visible light through a single-photon process and Ge(2) traps by a two-photon process. The de trapped electrons will diffuse through the core, until a photostationary distribution is developed. We consider a crude model in which such a Ge(1) charge distribution is established in the presence of the seed SHG field, which redistributes the Ge(1) centres by single photon absorption, The local Ge(1) population density is scaled by a factor $N/(1+I_p(r,\theta)/I_0)$, where $I_p(r,\theta)$ is the modal field intensity, I_0 is the saturation intensity for depopulation of the Ge(1) centres, and N is the normalisation factor which ensures conservation of the Ge(1) centres whithin the core. The redistribution is illustrated in Fig. 1, which plots the Ge(1) centres, the corresponding GeE' centre distribution and the resultant nett charge distribution arising from the separation of the Ge(1) and GeE' centres, for the case of HE_{21} seeding. In this case the electrons are pumped into the core centre.

The electrostatic field arising from this charge separation can be evaluated from solution of Poisson's equation. We denote the radial dependence of that field, which has the same azimuthal dependence as the transverse SHG field, by rd(r). The effective field for SHG is then found by the overlap of this field distribution with the second-harmonic field distribution. The complete details will be published elsewhere[13]. The mean field strength, at the peak of the interference, is given by

$$E_{dc} = (2\Delta)^{1/2}\, U/V\, \rho\, r_c\, S_{II'}\, e / \varepsilon$$

where ρ is the number density of Ge(1) centres in the core of radius r_c , ε is the dielectric permittivity of silica and $S_{II'}$ is the dimensionless overlap integral, of order unity, of the SHG field distribution with the electrostatic field distribution, given by

$$S_{II'} = (1+\delta(l)) \int_0^{r_c} r\, d(r)\ f_{l,t}(r)\, dr\ /r_c^2$$

We note that thermal relaxation of the electrostatic field is quite likely when the SHG light is absent. However, such a relaxation does not give rise to charge recombination because of the stress stabilisation described above. This rationalises the induction time observed for SHG in aged fibres.

c. SHG by the EFISH process.

The SHG occurs when the fibre is subject only to the pump fields. The electrostatic field generates SHG through the third-order susceptibility $\chi^{(3)}$. Thus

$$\chi_{xxx}^{(2)} = \chi_{xxxx}^{(3)} E_{dc} \eta_s^{1/2} \eta_p \cos((2\beta_p - \beta_s)z)$$

where η_s and η_p are the core fill factors of the SHG and pump modes.

EVALUATION

The model can now be quantitatively tested. We consider the case of SHG in the HE_{21} mode. The saturation number density of Ge(1) centres ρ can be estimated from the saturation number density of GeE' centres and the fraction of electrons released by their production which are trapped in Ge(1) centres. We find that $\rho = 2.3 \times 10^{16}$ cm^{-3}. The integral S_{10} was estimated to be 0.71. Thus the mean electrostatic field strength is estimated to be 80 V/μm for a 1μm radius core. For a fibre with $\Delta = 0.008$, we estimate an effective $\chi^{(2)}$ of 6.3×10^{-15} m/V, compared with the saturation value of 2.8×10^{-16} m/V measured experimentally.

The modal selection rules for SHG from this model are not strict. TE and TM modes do not posses longitudinal fields, wheras the HE and EH modes do. In most cases, we can find a longitudinal field component which provides the correct symmetry for SHG from the pump into that mode. The longitudinal field can be that of the seed. The relative efficiencies of HE and EH modes will depend on the overlap integral $S_{||}$. The polarisation of the modes is complicated by the bias of the response to x-polarisation. Thus the modes will be approximated by the LP description, with the dominant polarisation coincident with the pump. For the case of self-seeded SHG, the initial SHG generated through the quadrupolar interactions[21] will play a critical role because the selection rules are stronger. These results are in general agreement with experimental observations[17-20].

We conclude that the model gives good agreement with experiment. The most important feature is the symmetry breaking through an involvement of the longitudinal fields of either the pump or probe in the photoionisation of wrong bonds, stabilisation of these defects by stress relief and optical pumping of the electrons to produce a macroscopic field, which produces SHG by the EFISH process.

ACKNOWLEDGEMENTS

The authors with to thank Dr Martijn de Sterke and Dr Ian Bassett for their inputs. OTC Limited is acknowledged as sponsor of the Optical Fibre Technology Centre.

References

1. U. Osterberg and W Margulis, Opt. Lett. **12**, 57 (1987)
2. U. Ostergerg and W. Margulis, Opt. Lett. **11**, 516 (1986)
3. M. C. Farries, P. St. J. Russell, M. *E.* Fermann and D. N. Payne, *E*lectron. Lett. **23**, 322 (1987)
4. R. H. Stolen and H. W. K. Tom, Opt. Lett. **12**, 585 (1987)
5. R. H. Stolen, in *"Non-linear waves in Solid State Physics"*, A. D. Boardman, T. Twardowski and M. Bertolotti eds. (Plenum, NY, 1990)
6. P. St. J. Russell, L. J. Poyntz-Wright and D. P. Hand, SPIE Vol. **1373**, 126-139 (1990)
7. B. Lesche, J. Opt. Soc. Am. B**7**, 53 (1990)
8. D. A. Weinberger, A. Kamal and W. H. Weber, Opt. Lett. **15**, 613 (1990).
9. T. Tsai, M. A. Saifi, *E.* J. Friebele, D. L. Griscom and U. Osterberg, Opt. Lett. **14**, 1023 (1989)
10. D. A. Weinberger, OSA Annual Meeting technical digest, postdeadline paper PDP25, p58 (1990)
11. V. Mizrahi, Y. Hibino and G. Stegeman, ibid , technical digest, postdeadline paper, PD9-14 (1990)
12. D. Z. Anderson, Proc. SPIE **1148**, 186 (1989)
13. M. G. Sceats and S. B. Poole, (to be published)
14. A. W. Snyder and J. D. Love, *"Optical Waveguide Theory"* (Chapman and Hall, London, 1983) pp249
15. S. B. Poole and M. G. Sceats (to be published)
16. D. P. Hand and P. St. J. Russell, Opt. Lett., **15**, 102 (1990)
17. *H. Hibino, V. Mizrahi, G. I. Stegeman and S. Sudo, Appl. Phys. Lett.* **57**, 656 (1990)
18. B. Batdorf, C. Krautschik, U. Osterberg, G. Stegeman, J. W. Leitch, J. R. Rotge and T. F. Morse, Opt. Commun, **73**, 393 (1989)
19. U. Osterberg, R. I. Lawconnel, L. A. Brambani, C. G. Askins and *E.* J. Friebele, Opt. Lett. **16**, 132 (1991)
20. W. Henry, U. Osterberg, J. W. Leitch and J. R. Rotge, Proc. Photo-Opt Instrum. *E*ng. **1148**, 197 (1989)
21. F. P. Payne, *E*lectron. Lett. **23**, 1214-1215 (1987)

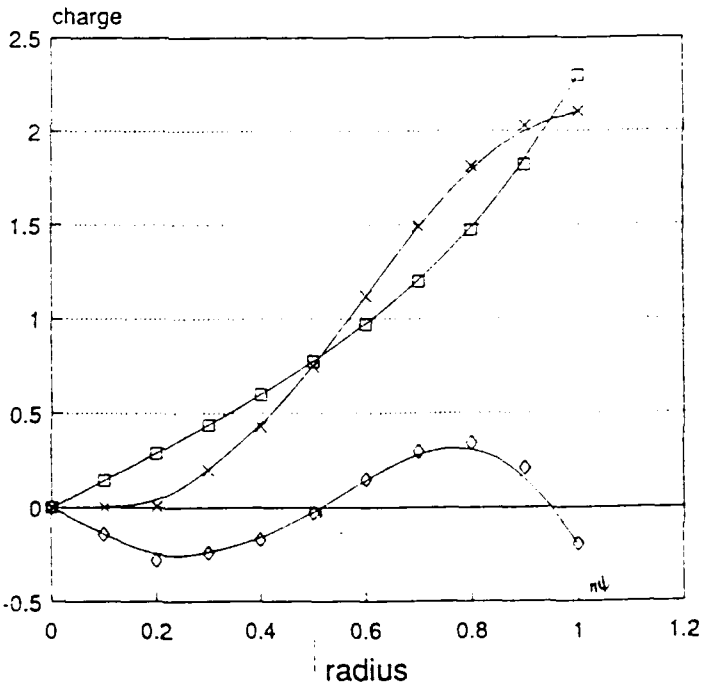

Figure Caption

Figure 1: The radial dependences of the positive *GeE'* centres (□), the optically pumped negative *Ge(1)* centres (×) and the nett charge (◇) for SHG in the HE_{21} mode from a pump in the HE_{11} mode are shown

Saturation of two-photon excited photoluminescence in Ge-doped fiber

Sophie LaRochelle, Alain Blouin, and François Ouellette
Centre d'Optique, Photonique et Lasers
Département de génie électrique, Université Laval
Québec (Québec), Canada, G1K 7P4

The photosensitivity of Ge-doped fiber allows the fabrication of useful devices like Bragg gratings or intermodal couplers. Nevertheless, the physical mechanism leading to a permanent refractive index change is still not well understood. It has been suggested that the bleaching of an absorption band at 245 nm plays an important role in the process. One signature of this absorption band is the photoluminescence emitted around 400 nm [1]. This photoluminescence can be excited by direct absorption of UV light, and this method has been used previously to characterize the 245 absorption band [1,2]. We show here that the luminescence can also be excited by two-photon absorption of light around 500 nm. By measuring the photoluminescence signal as a function of the input intensity, we have observed significant deviation from the expected quadratic dependence, indicating a saturation of the two-photon absorption. From our measurements, the saturation intensity can be deduced, and the two-photon absorption cross-section can be estimated.

In our experimental set-up, the argon laser light at 488 nm or 514 nm is mechanically chopped, and launched in the core of the fiber (Lightwave Technologies PMF500 single-mode fiber). The two-photon excited luminescence at 400 nm is collected on the side of the fiber, by a large N.A. lens, and sent through a monochromator and color filters, to remove completely the scattered excitation light. A photomultiplier detects the filtered light and the signal is processed by a lock-in amplifier. Fig. 1 shows the spectrum of the luminescence excited by 488 nm and 514 nm light. The signal is stronger with 488 nm excitation, although at longer wavelengths, both signal intensities are the same, indicating that more than one band may be responsible for the absorption [1]. Fig. 2

shows the luminescence signal at 400 nm as a function of the excitation intensity for both 488 nm and 514 nm excitation. The data show a significant deviation from the purely quadratic dependence expected for two-photon-induced luminescence, but can be fitted very well by a saturation function of the form:

$$I_l = \frac{\alpha(I_{ex}/I_s)^2}{1+(I_{ex}/I_s)^2}$$

The solid line indicates the theoretical fit obtained from this equation. From this fit, we obtained values of I_s of 5.98±0.16 MW/cm^2 at 488 nm and 9.6±0.25 MW/cm^2 at 514 nm. The difference in the values of I_s is expected since it also depends on the detuning from the center of the absorption line. If we assume that the 488 nm line is almost exactly resonant, then we find from these values of I_s that the 514 nm line is about one linewidth away from the line center.

We also measured the luminescence of the same fiber heated at 400 C in a high pressure hydrogen atmosphere. It was recently shown that this treatment enhances the photosensitivity of the fiber [3], as well as its absorption at 245 nm [1,2]. The saturation intensity was found to be smaller than in untreated fiber by about 40%. This means that either the two-photon absorption cross-section is larger, or the relaxation time of the luminescence level is longer. In either case, it shows that the presence of hydrogen modifies substantially the physical characteristics of the absorbing defects. Table 1 summarizes these results and also shows the relative photoluminescence intensity (proportional to α/I_s^2), normalized to the signal obtained with 488 nm excitation in an untreated fiber.

A similarly good fit to the experimental data can be obtained if one considers that the absorbing dipoles are perfectly oriented. The signal is then proportional to:

$$I_{pl} = \alpha \int_0^{\pi} \frac{(I/I_s)^2 \cos^4\theta \sin\theta d\theta}{1+(I/I_s)^2\cos^4\theta}$$

The value of I_s obtained in this case is smaller by about 1.52. This is because an average is made between the dipoles of different orientations that are more or less easy to saturate.

To get an estimate of the two-photon absorption cross-section (TPAC), we assume that most of the excited electrons accumulate on the upper luminescence level, which is known to be a metastable level of lifetime $\tau \approx 80\mu$sec. The TPAC is then given by:

$$\sigma = \hbar\omega/\tau I_s^2$$

Using our measured values of I_s, we obtain cross-sections of the order of 10^{-30}-10^{-31} cm^4/W. Better estimates of the TPAC would require a precise measurement of the luminescence lifetime. Still, the measurement of the saturation intensity provides a simple but powerful tool for characterizing the UV absorption band.

One goal of this experiment was to measure the diminution of the photoluminescence signal as the fiber is exposed to a high intensity for a long time. This would confirm that the absorption band is indeed bleached out. However, even after prolonged exposure, no noticeable change in the signal could be detected, although the rather poor signal to noise ratio did not allow us to detect a change of less than about 5%. It remains to be seen whether such a small bleaching of the absorption band could account for the permanent index change close to 10^{-4} observed in photosensitive fiber.

References

1- M. Kohketsu, K. Awazu, H. Kawazoe, and M. Yamane, Jap. J. Appl. Phys. **28**, p.622, 1989.

2- D.M. Krol, R.M. Atkins, and P.J. Lemaire, 'Photoinduced second-harmonic generation and luminescence of defects in Ge-doped silica fibers', Int'l Workshop on Photoinduced Self-organization in Optical Fiber, Proc. SPIE **vol. 1516**, to be published (1991).

3- F. Ouellette, D. Gagnon, and M. Poirier, Appl. Phys. Lett. **58**, p.1813, 1991.

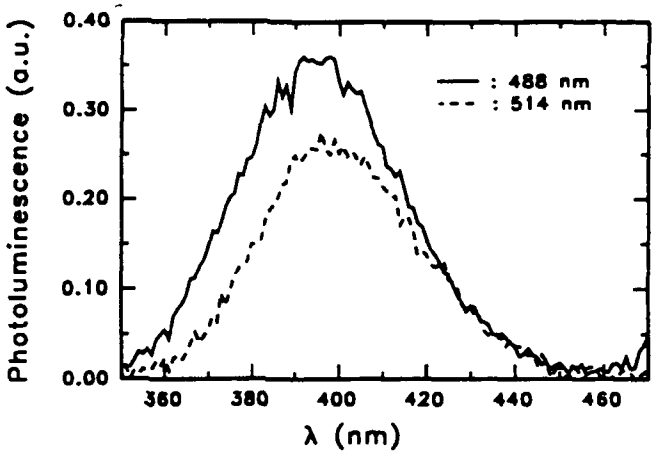

Fig. 1: Photoluminescence spectrum for the two excitation wavelengths (488 nm and 514 nm).

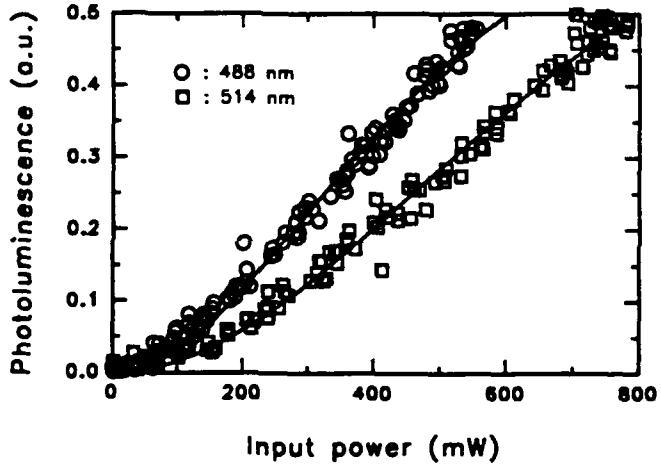

Fig. 2: Photoluminescence signal as a function of input power for 488 nm and 514 nm excitation. Solid lines: theoretical fit.

	488nm		514nm	
	α/I_s^2	I_s(MW/cm²)	α/I_s^2	I_s(MW/cm²)
untreated	1.0	5.98	0.47	9.60
H_2-treated	1.57	3.36	0.76	6.50

Table 1: Relative signal intensity and saturation intensity for excitation at 488nm and 514nm in untreated and H_2-treated fiber

Interference between photon echoes in an Er-doped fiber

V.L. da Silva, Y. Silberberg, J.P. Heritage, and E.W. Chase

Bellcore, 331 Newman springs Road, Red Bank, New Jersey 07701-7040
Tel: (908) 758-3130, FAX: (908) 741-2891

We report the observation of a new interference phenomenon in photon echo experiments which are performed in an optical fiber. This phenomenon is unique to the guided wave environment and is the result of propagation in an optically thick absorber. The use of optical fibers allows long interaction lengths where the propagation of the excitation pulses as well as the echoes is important.

In our experiment we have measured the shape of the second-order echo generated in an Er-doped fiber. We have found that below a certain power level the second order echo is double-peaked, and that at higher power levels it resumes its expected single peak shape. We attribute this phenomenon to an interference between two echo pulses generated through different mechanisms, as explained below.

We have used a modified version of the accumulated photon echo experiment described in [1]. A Michelson interferometer was used to generate a pair of delayed pulses from a NaCl:OH^- color-center laser with additive-pulse mode-locking. This pulses were spectrally filtered and then amplified in an Er-doped fiber pumped by a second color-center laser. The spectral filter and fiber amplifier combination assures that the amplified pulses spectrum is matched to the absorption line of the Er-doped fiber. Furthermore, as the amplifier is operated in the saturation regime, the output pulses are not sensitive to small fluctuations in the additive-pulse mode-locked laser. The amplified pulses were 0.8 psec long and had 76 W peak power. They were coupled to a 4.5 m long piece of Er-doped germanium-calcium-aluminum silicate fiber which was coiled to a 4 cm diameter, spliced to dispersion-shifted fiber pigtails and immersed in liquid helium.

The total average power coming out of the amplifier was 10 mW, which was enough to saturate the absorption from 45 dB to less than 5 dB. Under this excitation condition we could observe up to three orders of echo, as can be seen in fig. 1. This figure shows the cross-correlation of a delayed pulse from the color-center laser with the output from the cooled fiber.

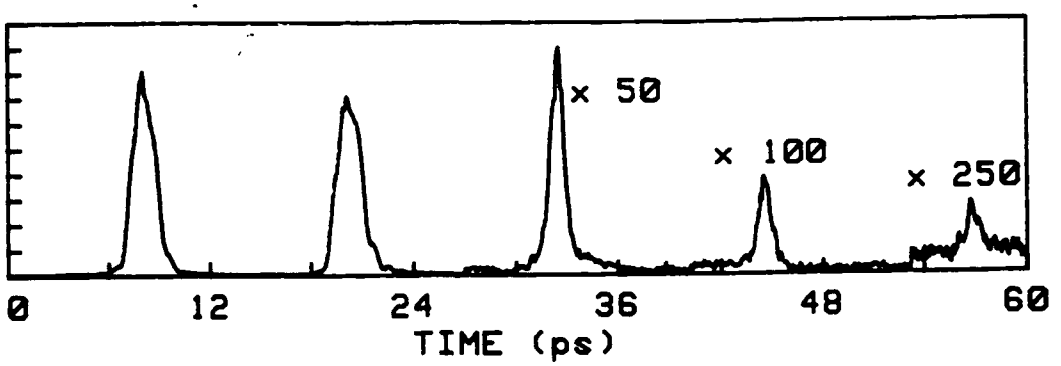

Figure 1. Cross-correlation of the output from the cooled Er-doped fiber.

We introduced a fiber attenuator between the fiber amplifier and the cooled Er-doped fiber in order to investigate the accumulated photon-echo behavior as a function of the excitation intensity. The first echo pulse increases with the excitation power until it saturates at ~ 0.3 mW of transmitted power. The second echo pulse, however, evolves differently. Figure 2 shows its cross-correlation for several power levels. Below 0.4 mW the second echo is double-peaked. As the power is increased, the valley between the peaks decreases until it completely disappears. From there on, the second echo pulse has a single-peaked shape and it grows with the excitation power.

Photon echoes can be described as diffraction orders on a frequency grating saturated into the absorption spectrum of an inhomogeneously broadened absorber [1]. In this model the second order echo is the result of the second order of diffraction of the second excitation pulse on that absorption grating. However, in an optically thick medium, the first order echo diffracts on the same grating, and its first order diffraction coincides with the second echo. It can be shown that the signal induced by the first echo, which is generated by two consecutive $\chi^{(3)}$ processes, is of the same order of magnitude as the $\chi^{(5)}$ process leading to the true second order echo. The two terms have opposite signs, and therefore interfere destructively to form a double-peaked pulse. A model calculating the shape of the second order echo agrees well with the experimental results, as shown in Fig. 3. Note that the echo interference phenomenon described above is the result of having an optically thick medium. Additional interference phenomena are expected to occur when nonlinear phase shift due to the Kerr effect in the fiber becomes of order π. The interplay between coherent effects and self-phase modulation can lead to a rich variety of phenomena which we are currently investigating.

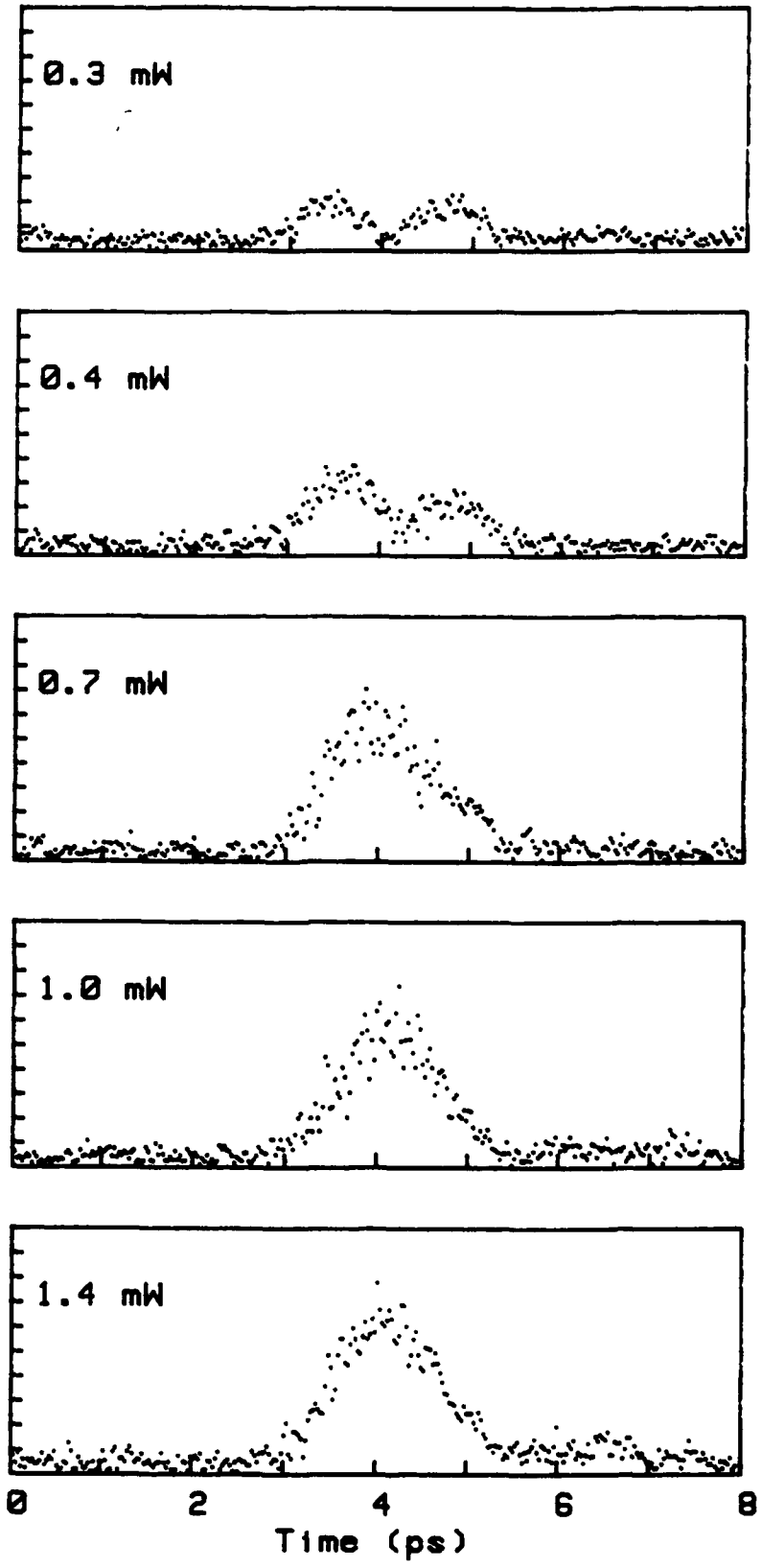

Figure 2. Cross-correlation of the second order echo pulse for several transmitted powers.

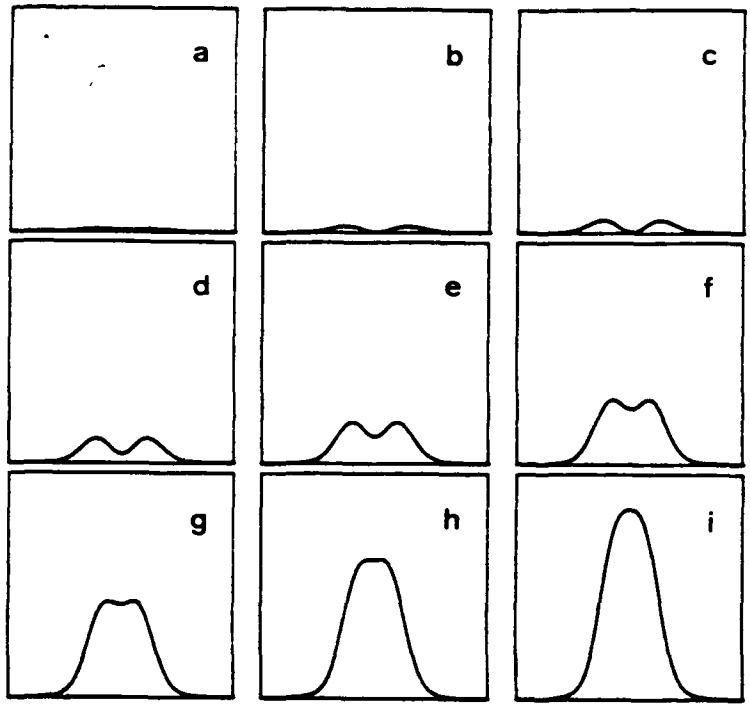

Figure 3. Second order echo pulse shape for several excitation intensity. (a) I = 2.0 Is, (b) I = 2.5 Is, (c) I = 3.0 Is, (d) I = 3.5 Is, (e) I = 4.0 Is, (f) I = 4.5 Is, (g) I = 5.0 Is, (h) I = 5.5 Is, (i) I = 6.0 Is. Is is the saturation intensity.

In conclusion, we have studied the accumulated photon-echo in an Er-doped fiber in the regime of strong absorption saturation. We have measured up to the third echo and observed, for the first time, significant changes in the shape of the second echo as a function of the excitation intensity. We have developed a theoretical model that describes the accumulated photon-echo in the strong saturation regime that predicts the behavior of the second echo.

References

1. Y. Silberberg, V.L. da Silva, J.P. Heritage, E.W. Chase, M.A. Saifi, M.J. Andrejco, "Coherent effects in Er-doped fibers: photon echo with femtosecond pulses", Topical Meeting on Nonlinear Guided Wave Phenomena, Cambridge, England, paper TuA1.

PASSIVE, ALL-FIBRE SOURCE OF FUNDAMENTAL, FEMTOSECOND SOLITONS

D.J.RICHARDSON, A.B. GRUDININ* AND D.N. PAYNE
OPTOELECTRONICS RESEARCH CENTRE
UNIVERSITY OF SOUTHAMPTON
S09 5NH, UK

Advances in erbium-doped fibre fabrication and the generation and amplification of ultra-short pulses [1-5] make the development of sub-100 fs pulse sources based on erbium-doped fibre a very attractive proposition.

Recently, a source of 320 fs pulses from a passively mode-locked fibre laser has been reported [4,5]. Despite the very broad gain-bandwidth of erbium ions in silica, the effect of soliton self-frequency shift (SSFS) restricts the minimum possible pulse duration to around 300 fs. One possible way to make shorter pulses is to exploit the pulse compression effects which occur during soliton amplification in a fibre amplifier [3]. In this paper we report the results of an experimental study of both the temporal and spectral characteristics of pulses generated within an all-fibre unit containing a passive erbium-doped fibre laser, an erbium doped amplifier and a short section of undoped dispersion-shifted fibre.

The experimental configuration is shown in Fig.1. The performance of the passively mode-locked laser has been described elsewhere [4]. With just 20 mW of launched pump power at 980 nm, a power easily obtainable from a laser diode, the laser produces bandwidth-limited soliton pulses with a duration of 500 fs or less. The average output power in this instance was 120 μW. The external amplifier consisted of 5.5 m of erbium-doped fibre (NA= 0.15, λ_{co} = 1230 nm) with an Er^{3+}-doping level of 800 ppm. With an amplifier pump power of 200 mW a gain of 25 dB was obtained and pulse compression down to 90 fs was observed at the fibre output (see Fig.2). In addition to the compression, note the spectral shift due to the Soliton Self Frequency Shift (SSFS)[6] in the spectra in Fig.2. The time-bandwidth product for these pulses is 0.3, in reasonable agreement with that expected for a $sech^2x$ pulse shape. Thus, during soliton amplification and propagation we have transformed 500 fs fundamental solitons at 1.56 μm into 90 fs fundamental solitons at 1.59 μm. At higher amplifier gains, high-order soliton break-up into coloured solitons due to SSFS was observed, the individual pulse widths being of the order 100 fsec.

* On leave from: Optical Fibre Department, General Physics Institute, USSR Academy of Sciences, 117942 Moscow.

The amplifier length was reduced to 4.5 m in order to reduce the SSFS at the amplifier output and the amplifier pump adjusted slightly to enable us to obtain the shortest possible, single, high-order soliton pulse, as shown in Fig.3. A 1.2 m length of dispersion-shifted fibre was then spliced to the amplifier output in order to obtain further pulsewidth reduction by high-order soliton compression.

The dispersion of the fibre was 1.5 ps/nm/km within the 1.55-1.61 μm wavelength range. At the propagation "focal point" within the undoped fibre, the pulse duration is comparable to the Raman response time. We therefore expect SSRS to have a great influence on the pulse evolution. The SSRS results in both temporal and spectral separation of the short central spike from the rest of the pulse, yielding compressed pulses at the output of the dispersion-shifted fibre. Using this technique we have obtained fundamental solitons as short as 50 fs at 1.59 μm (Fig.4a). With increased amplifier pump power we observed coloured soliton generation as shown in Fig.4. At 270 mW pump input we observed the appearance of a second pulse (Fig.4b) and at 320 mw and 350 mW additional soliton pulses became apparent (Fig.4c,d).

In conclusion, we have demonstrated for the first time an all-fibre module capable of generating 50 fs fundamental solitons within the 1.6 μm region with repetition rates as high as 1GHz. We envisage being able to generate pulses as short as 20 fs. Results of further investigations into the properties of such a pulse source, including detailed measurements of coloured soliton generation, will be presented at the conference.

Acknowledgements: The Optoelectronics Research Centre is supported by the U.K. Science and Engineering Research Council

References.

1) M.E.Fermann, M.Hofer, F.Haberl, A.J.Schmidt, and L.Turi, Opt.Lett., 16, 244, (1991)

2) A.S. Gouveia-Neto, A.S.L. Gomes and J.R. Taylor: Opt. Lett., 14, 514, (1989)

3) I.Y.Khrushchev, A.B.Grudinin, E.M.Dianov, D.V.Korobkin,Jr., V.A.Semenov, and A.M.Prokhorov, Electron.Lett., 26, 456, (1990)

4) D.J.Richardson, R.I.Laming, D.N.Payne, M.W.Phillips, and V.J.Matsas, Electron. Lett.,27, 730, (1991)

5) E.M. Dianov et al.: JETP Lett., 41, 242, (1985).

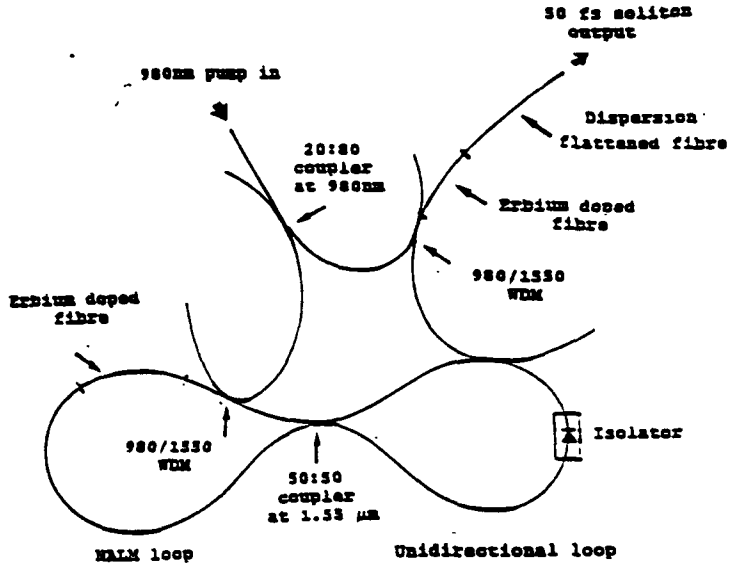

Fig.1 All-fiber circuit

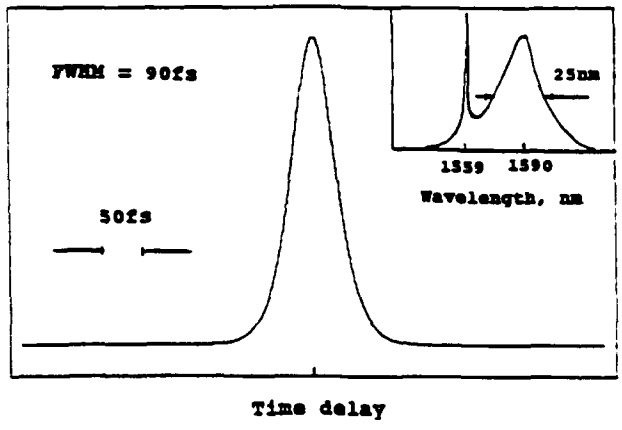

Fig.2 Background free autocorrelation trace and spectrum of 90fs pulses at output of 5.5m fibre amplifier. Amplifier pump power - 200mW

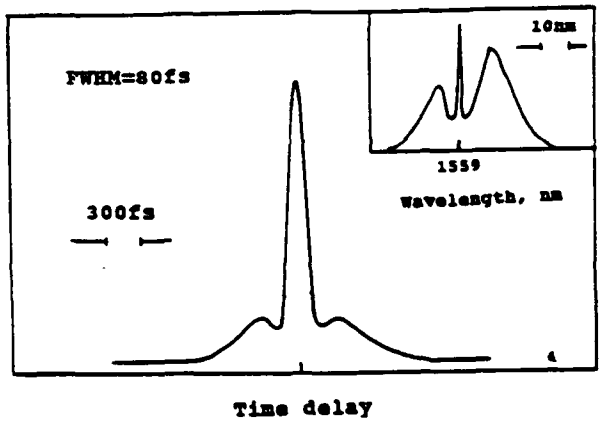

Fig.3 Background free autocorrelation trace and spectrum of 80fs pulses at output of 4.5m fiber amplifier. Amplifier pump power - 200mW

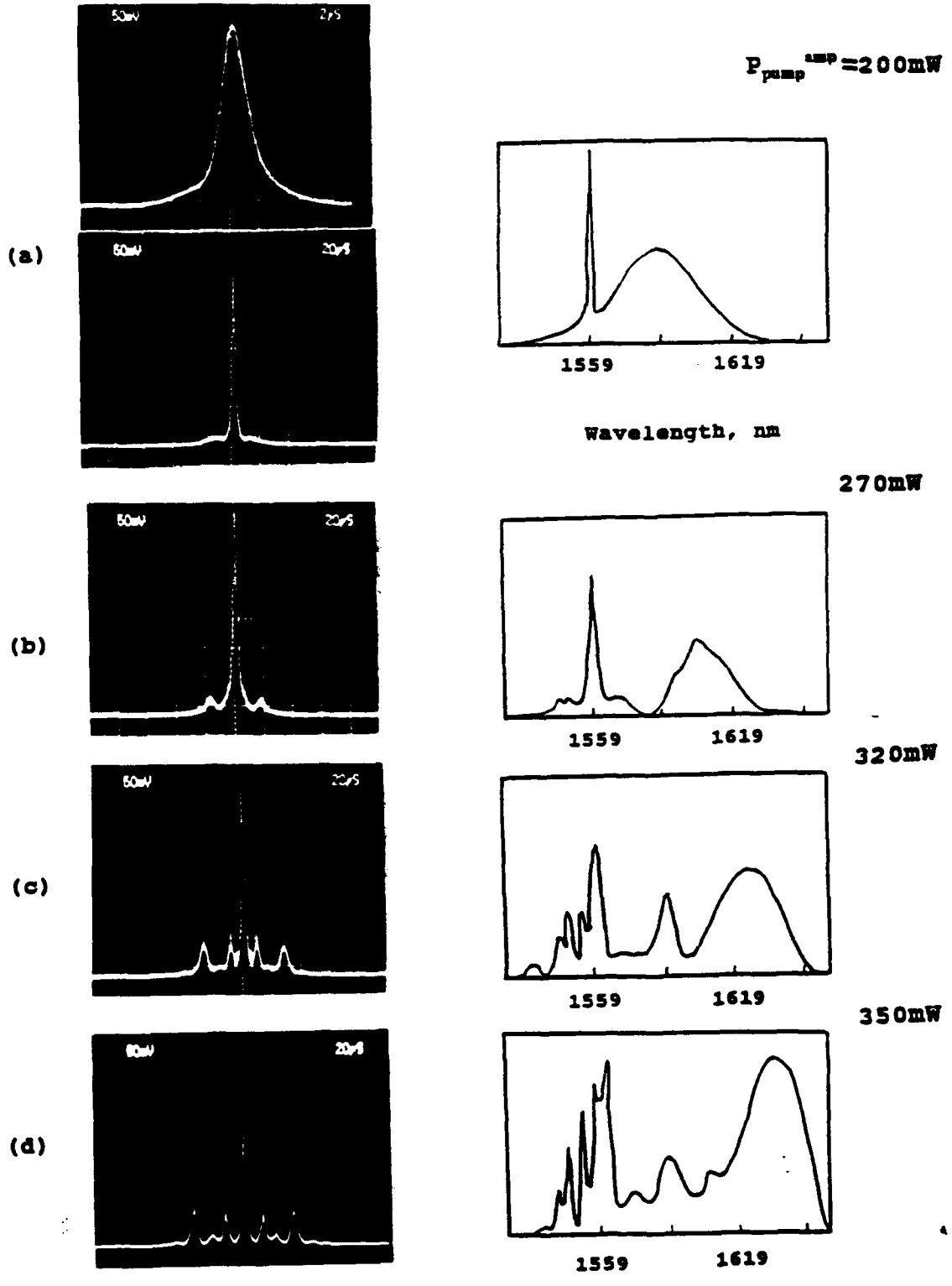

Fig.4 Real-time autocorrelation traces and spectra at the system output for various amplifier pump powers. (a) represents a 50fs fundamental soliton

Repetition rate control of an LD-pumped femtosecond erbium-doped fiber laser using a sub ring cavity

by

Masataka Nakazawa, Eiji Yoshida, and Yasuo Kimura
Nonlinear Optical Transmission Media Research Group
NTT Optical Transmission Line Laboratory
Tokai, Ibaraki-ken 319-11
Japan

With a view to generating femtosecond pulses from lasers, an additive pulse modelocking (APM) technique has recently been developed, in which a nonlinear Fabry-Perot cavity plays an important role in narrowing the output pulse by using interference.[1] The pulse operation mechanism of the laser can be classified as fast saturable absorber modelocking. An alternative way to obtain nonlinear interference is to use an optical fiber loop instead of the nonlinear Fabry Perot fiber cavity. Doran and Wood presented an interesting idea for switching the pulse which is accompanied by simultaneous pulse shaping, the so called nonlinear optical loop mirror (NOLM).[2] Fermann et al. presented a modified NOLM, which is called the nonlinear amplifying loop mirror (NALM).[3] An EDFA is installed inside the loop mirror which is terminated by a 50 : 50 coupler. Thus, low threshold switching can be realized in the NALM.

Recently, Duling[4] and Richardson et al.[5] reported very interesting results for femtosecond~picosecond pulse generation from erbium-doped fiber lasers with a NALM, and a theoretical investigation of a pulse laser with a NOLM was also reported.[6] We also succeeded in generating a 290 fs femtosecond pulse from an erbium-doped fiber laser with a NALM pumped by InGaAsP laser diodes.[7] However, it was very difficult to control the repetition rate of the output pulse. In the present paper, we will report for the first time, a repetition-rate controlled low-threshold femtosecond erbium-doped fiber laser with a NALM pumped by InGaAsP laser diodes. This is achieved by attaching a sub ring cavity.

The experimental setup for the femtosecond erbium-doped fiber laser is shown in Fig. 1. The laser had a NALM and a linear loop to recirculate the switched pulse through a polarization-insensitive optical isolator. A sub ring cavity was attached to the linear loop to control the repetition-rate of the output pulse. The transit time of the pulse in the main cavity was equal

to an integer of that in the sub ring cavity. An EDFA was installed in the linear loop in order to compensate for the insertion loss of the sub cavity. The NALM consisted of a 50: 50 fiber coupler, an erbium-doped fiber, a fiber coupler to pump the EDFA, and a dispersion-shifted fiber for nonlinear phase change. The output pulse was extracted through a 30 % fiber coupler in the linear loop. The erbium-doped fiber, located asymmetrically within the NALM, had a length of 10 m and a doping concentration of 630 ppm with a 4000 ppm Al_2O_3-codoping. The modefield diameter, cut-off and zero dispersion wavelengths were 5.6 μm, 1.2 μm, and 1.53 μm, respectively. The pumping source was InGaAsP laser diodes with a central wavelength of 1.48 μm. Polarization controllers (P. C.) were installed in both loops to control the oscillation modes (Modelocking or Q-switching) and to initiate pulse oscillation when the laser did not oscillate.

The output power of the fiber laser vs. the launched pump power is shown in Fig. 2, in which the nonlinear fiber in the NALM was 30 m and the GVD was - 0.8 ps/km/nm. The total loop length was 60.8 m, resulting in a fundamental repetition rate of 3.29 MHz. The length of the sub ring cavity was 1.60 m. Thus, a repetition rate increase of 38 times can be expected.

There are three characteristic areas in the operation. One is the Q-switch operation region, in which the laser operates in a self-starting Q-switch mode with a repetition rate of 125 MHz, which is determined by 3.29(MHz)x38=125 MHz. This mode was obtained at a relatively high pump power of larger than 30 mW. The second is operation in a modelocked condition in which the repetition rate of the output pulse can be stably controlled by tuning the sub ring cavity length. This mode was obtained at a pump power of 30~20 mW. Typical output power was 0.7~0.8 mW. The third is also operation in a modelocked condition, but the repetition rate was unfixed. The repetitive pulses sometimes disappeared. This operation was achieved in the relatively low pump power region of less than 20 mW, and the modelocking was maintained even with a pump power of as low as 10 mW.

It is important to note that once the modelocked condition is stopped by decreasing the pump power, lasing does not resume unless the pump power is increased to around 50 mW. Therefore, the system exhibits pump power hysteresis. This means that a low pump power cannot initiate the system, which is quite understandable since a low pump power cannot sustain sufficient energy in the cavity for nonlinear switching.

The experimental results for the repetition rate control of the output pulses are shown in Fig. 3. It is clearly seen in (a) and (b) that a uniform repetition rate was achieved. It is important to note that the repetition rate can be controlled, but amplitude still changes with time as shown in (b). The average output power of 0.7 mW and the pulse width of 315 fs give a peak power of 17.8 W. The pulse width measured with an autocorrelator was about 315 fs and the spectral width was 8.2 nm. Thus, $\Delta\nu\Delta\tau$ of the output pulse is approximately 0.32, which means that the pulse is a transform-limited sech pulse. On the other hand, the N=1 soliton power for a GVD of -0.8 ps/km/nm at an oscillation wavelength of 1.56 μm, a pulse width of 315 fs, and a spot size of 4 μm is about 12.6 W, which almost agrees with the experimental result. Thus, the output pulses are optical solitons. Although the repetition rate is neatly fixed, the amplitude of the pulse varies with time. Without attaching a sub ring cavity, the modelocked pulses bunched together and the repetition rate was not fixed. Waveforms (c) and (d) show the output pulses when the length of the sub ring cavity is detuned from an inverse of an integer of the main cavity length. Here the repetition rate is not uniform. However, the pulse width measured with an autocorrelator did not change even in the detuned condition.

In summary, we have presented a simple method for controlling the repetition rate of a femtosecond erbium-doped fiber laser with a NALM by attaching a sub ring cavity. Although it is not easy to obtain constant amplitude output pulses, the repetition rate can be completely controlled.

Reference

[1] J. Mark, L. Y. Liu, K. L. Hall, H. A. Haus, and E. P. Ippen, Opt. Lett., **14**, 48 (1989).

[2] N. J. Doran and D. Wood, Opt. Lett., **13**, 56 (1988)., see also J, Opt. Soc. Ame. B, **4**, 1843 (1987), and see also J. D. Moores, K. Bergman, H. A. Haus, and E. P. Ippen, J. Opt. Soc. Ame. B, **8**, 594 (1991).

[3] M. E. Fermann, F. Haberl, M. Hofer, and H. Hochreiter, Opt. Lett., **15**, 752 (1990)., see also D. J. Richardson, R. I. Laming, and D. N. Payne, Electron. Lett., **26**, 1179 (1990).

[4] I. N. Duling, III, Electron. Lett., **27**, 545 (1991)., see also Opt. Soc. Ame. Annual Meeting, (Optical Society of America, Washington DC), PDP4, 306 (1991).

[5] D. J. Richardson, R. I. Laming, D. N. Payne, M. W. Phillips, and V. J. Matsas, Electron. Lett., **27**, 731 (1991), see also Electron. Lett., **27**, 543 (1991).

[6] A. G. Bulushev, E. M. Dianov, and O. G. Okhotnikov, Opt. Lett., **16**, 88 (1991).

[7] M. Nakazawa, E. Yoshida, and Y. Kimura, Appl. Phys. Lett., to be published in Oct. 21 issue, (1991).

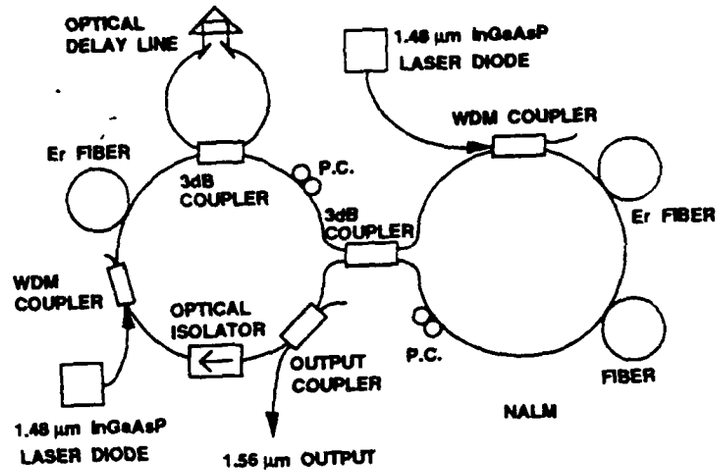

Figure 1 Experimental setup for the repetition rate controlled femtosecond erbium-doped fiber laser. The pumping source is 1.48 μm InGaAsP laser diodes.

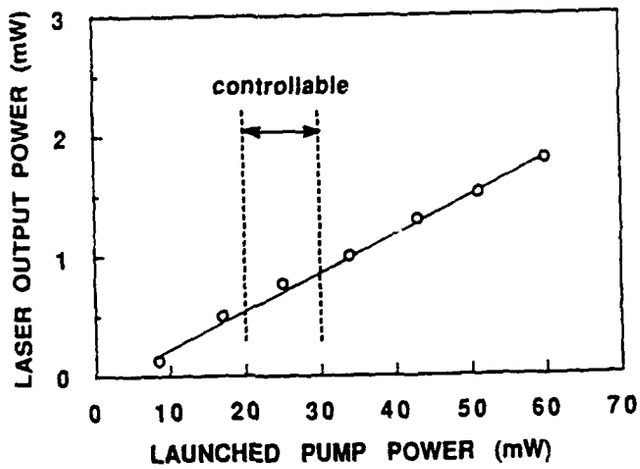

Figure 2 Output power vs. the launched pump power of the laser.

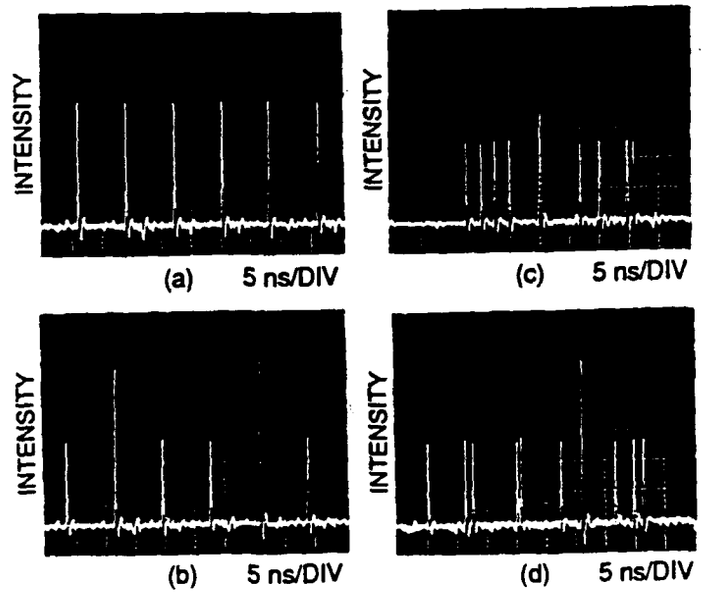

Figure 3 Repetition-rate control of output pulses in a modelock operation mode. The repetition rate was controlled in (a) and (b). (c) and (d) show output pulses when the length of the sub ring cavity was detuned by + 1.5 mm from the inverse integer of the main cavity length.

A Digital Nonlinear Optical Loop Mirror Switch

N. Finlayson, B.K. Nayar and N. J. Doran
BT Laboratories, Martlesham Heath, Ipswich IP5 7RE.

Ultrafast all-optical switching has been demonstrated in a number of silica fibre interferometric devices. In particular, the nonlinear optical loop mirror (NOLM), first fabricated by us, has been successfully used to demonstrate stable ultrafast multiplexing/de-multiplexing for high bit-rate optical fibre communication systems and for pulse shaping and pedestal supression. The switching power tends to be generally high due to the small nonlinearity of fused silica. However, the signal switching powers can now be reduced to the order of microwatts with the use of fibre amplifiers due to demonstrably stable operation of NOLMs with very long loop lengths (> 5 km). The NOLM exhibits a sinusoidal CW transmittance as a function of the input power. The development of an ultrafast *digital* optical switch for all-optical signal processing is attractive [1], requiring that the switching characteristics be sharper than sinusoidal. One approach to synthesizing a digital switching characteristic is to concatenate nonlinear fibre interferometric switching devices. In this paper we present the results of the first switching experiment involving two concatenated NOLMs. Digital switching characteristics are obtained. The device can also be used for generating nearly square pulses.

The theoretical gains that can be achieved by concatenating nonlinear optical switching devices are considerable, as shown in Fig. 1. Sigmoid power-dependent characteristics are obtained which are suitable for performing all-optical logic operations. It is evident that substantial improvement is obtained when as few as two devices are concatenated. In order to minimise the component count and ensure matching of the characteristics of successive NOLMs we have employed a novel double-pass design to realize a digital switching characteristic. The experimental configuration is shown in Fig. 2. The device consists of a single NOLM with a linear fibre loop mirror spliced at the output. The linear mirror can be configured to perfectly reflect all incoming light back through the NOLM. A fibre polarisation controller placed between the NOLM and the linear mirror ensures that the double-pass signal through the NOLM has an orthogonal polarisation to that of the single-pass signal. A polarising beam splitter at the output port is then used to separate the single-pass and double-pass signals, effectively converting a two terminal device into a three terminal device.

The CW transmittance, $T^{(2)}$, of two concatenated NOLMs in absence of losses is given by:

$$T^{(2)} = T^{(1)}\left\{1-2\alpha(1-\alpha)\left[1+\cos(1-2\alpha)\phi_{NL}T^{(1)}\right]\right\}$$

where the CW transmittance of the first NOLM is $T^{(1)} = 1-2\alpha(1-\alpha)\left[1+\cos(1-2\alpha)\phi_{NL}\right]$. The power splitting ratio of the coupler is α:/(1-α) and $\alpha \neq 0.5$; $\phi_{NL} = (2\pi/\lambda)n_2 l(P_i/A_{eff})$ is the nonlinear phase change; l is the wavelength; n_2 is the intensity dependent refractive index which for silica fibres has a value $3.2\text{x}10^{-20}$ m^2W^{-1}; l is the effective fibre length; P_i is the input power; and A_{eff} is the effective mode area. The theoretical power-dependent transmittance functions for a single NOLM and two concatenated NOLMs is shown in Fig. 3 (a). The corresponding experimental results are shown in Fig. 3(b). Considerable sharpening of the characteristic is obtained with the two gate device, and excellent agreement is obtained with theory.

Pulse-shaping effects were monitored with fast InGaAs photodiodes along with a 40 GHz Tektronix sampling head. In Fig. 4 (a) the temporal response of single-pass reflected and double-pass transmitted pulses is given for $P_i = 0.85\text{x}P_\pi$, where P_π is the peak input power required for switching single-pass NOLM from the reflecting to transmitting state i.e. satisfying the condition $(1 - 2\alpha)\phi_{NL} = \pi$. The double-pass transmitted pulse has width 62 ps (FWHM) compared with an input laser pulse width of 125 ps (FWHM). The reflected pulse exhibits a corresponding double peaked characteristic. An application of the double-pass NOLM is in pulse shaping to produce square or near-square pulses. The transmitted pulse will have an optimum "square" temporal profile for P_i slightly greater than P_π and it can be theoretically shown that this occurs for $P_i = 1.2\text{x}P_\pi$ independent of α. In Fig. 4 (b) the temporal response of the double-pass pulse corresponding to this power is given. The pulse width is 100 ps (FWHM) and the temporal shape is significantly squarer than the Gaussian input pulse shape.

In conclusion, we have demonstrated for the first time the synthesis of a digital switching characteristic by concatenation of nonlinear fibre interferometric devices. A novel configuration is used which minimises the component count and results in three terminal operation of the device. This switch can be used as a fundamental gate in ultrafast pipeline all-optical processing architectures. In addition, it has been shown that this device can be used to produce square pulses.

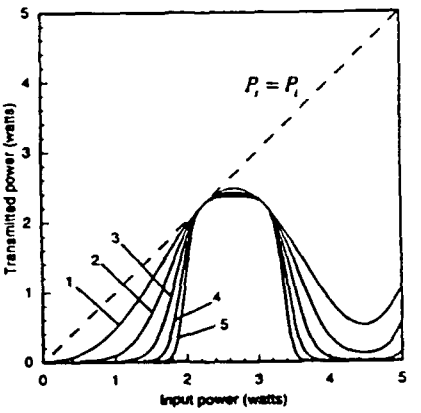

Fig. 1 Theoretical effects of loop mirror concatenation.

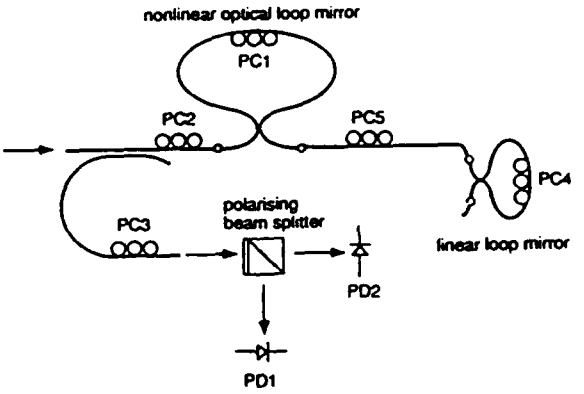

Fig. 2 Experimental setup.

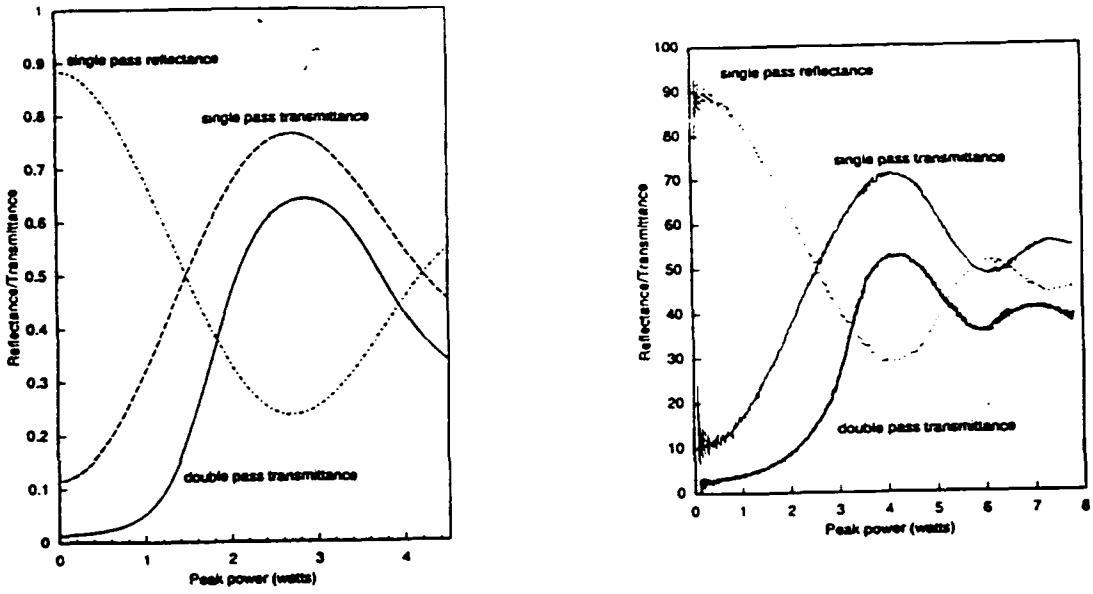

(a) (b)

Fig. 3 Comparison of theoretical and experimental characteristics of a double-pass nonlinear optical loop mirror (a) theory (b) experiment.

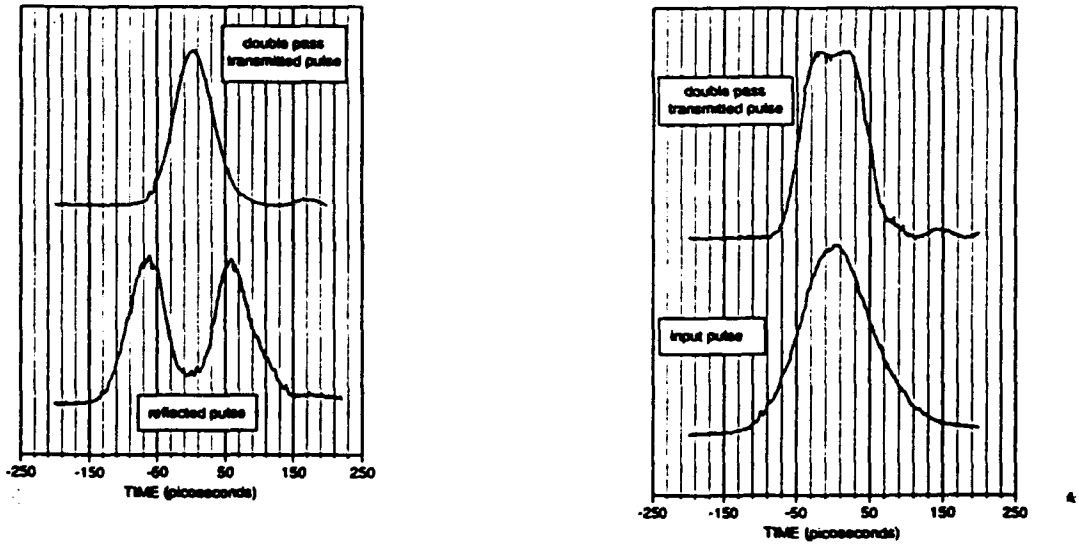

(a) (b)

Fig. 4 Pulse shaping effects in the double pass NOLM. (a) transmitted and reflected pulses at peak transmittance (b) input and transmitted pulses at slightly higher power.

All-optical, all-fiber circulating shift register with inverter

N. A. Whitaker, Jr., M. C. Gabriel, H. Avramopoulos, A. Huang
AT&T Bell Laboratories, Holmdel, NJ 07733

An all-optical fiber-Sagnac interferometer switch and erbium amplifier have been combined to demonstrate a 254 bit circulating shift register with an inverter.

All-optical information processing using an ultrafast effect such as the optical Kerr effect holds promise for processing throughput rates which are faster than electronics. To build a cascadable, optical three-terminal device, a control beam must be used which is isolated from a separate signal beam. Fiber Sagnac interferometer switches[1] have been shown to be good candidates for all-optical processing. Two distinct optical wavelengths can be used [2-5], in which case lossless combination and separation of the control and signal can be effected using wavelength dependent couplers or filters. Recently a polarization-based switch was demonstrated [6,7], in which polarization rather than wavelength was used to distinguish the control beam from the signal beam. Identical devices with polarization discriminated inputs are capable of being cascaded, as demonstrated in the experiment described here.

Configuring a Sagnac loop as a three-terminal switch [6,7], a control beam is introduced asymmetrically into the loop, so as to travel in one direction only. The signal beam is split into two equal beams, which traverse the Sagnac loop in both directions and recombine interferometrically. The signal beam is held in a single linearly polarized state in the loop, and the control beam is introduced in an orthogonal state using a polarization combining coupler. When the control beam is absent, the recombining signal beams interefere at the coupler so that the pulse is reflected back into the input port of the interferometer. With the control beam present, a nonlinear phase shift on the half of the signal beam with which it co-travels causes the pulse to be transmitted rather than reflected. For this demonstration, the reflected output of a Sagnac loop switch (which is the logical inverse of the control signal) is amplified and fed back to provide the control signal after a time delay. This configuration implements the circulating shift register with inverter shown in Figure 1. The length of the shift register is determined by the time between pulses, and the time it takes the light to traverse the entire circuit. The clock in this case is provided by the pulsed laser, and the power supply is provided by the erbium amplifier.

The experimental apparatus is shown in Figure 2. The signal pulses were generated from a synchronously pumped KCl:Tl F-center laser (FCL), pumped by a modelocked Nd:YAG laser at 100 MHz. Autocorrelation showed the pulsewidths to be approximately 15 ps. The wavelength was set at 1531.6 nm which was close to the gain peak of the amplifier. After the light was coupled into the fiber, a 43:57 coupler was used both to monitor the light from the FCL, as well as to extract the reflected signal which was amplified to form the control beam. The reflected signal is amplified in an erbium-doped fiber amplifier, pumped at 528nm as described earlier [7].

The loop is formed from polarization maintaining fiber (PMF). The polarization maintaining coupler (PMC) which is used to form the Sagnac interferometer has a coupling ratio which is nominally 3 dB. The polarization combining coupler (PBS1) and the polarization splitting coupler (PBS2) are used to couple the control beam into and out of the loop. With ideal components this makes possible lossless combination and perfect isolation of the control and signal beams. The length of the loop itself is approximately 450 meters, consisting of 9 sections which are 50 ± 5 m in length, separated by 8 crossed-axis splices. This corresponds to approximately 96 ± 10ps of slip in each section. These splices allow the control pulse and signal pulse to multiply interact [7,8], and provides other benefits such as jitter independence, removal of coherence problems,

and pulse shape tolerance[7]. Although the transmission through the series of crossed-axis splices is approximately 90%, the reflectivity of the Sagnac at low power is approximately 3 dB due to losses at the splices between the couplers and the PMF.

The polarization controllers were set by first blocking the pump to the EDFA, and using the PC1 to minimize the power which leaves the system at DMP. This puts the polarization of the input light on the signal axis of the Sagnac loop. The amplifier is then unblocked, and PC2 is used to minimize the output power through the DMP port, which this time is mostly control power. This procedure puts all available power from the amplifier on the control axis of the Sagnac loop.

When the system is started, there is no control light in the loop, so the system is initially reflective. The reflected pulses are amplified, and 254 pulses are reflected before the first reflected pulse reaches the PBS1 coupler. The reflected pulse co-travels the loop with the 255th signal pulse, and shifts its phase enough to cause it to leave the system by the TO port, rather than to be reflected. Thus no reflected pulse is generated, and the initial conditions are restored. The 255th through 508th pulses are transmitted, and the 509th pulse again transits the loop without a control signal so is reflected once again. While all the light which enters the system transits the loop twice, once as the signal beam and once as the control beam, the system retains the information about the initial state. Thus this system also demonstrates a fiber loop memory.

Figure 3a shows the resulting envelope of pulses which was observed at the CNTLO port on a detector. The measured period is 5.08 μs, which is twice the delay of the loop. The circuit could function stably for hours, until the polarization of the non-polarization-holding parts of the circuit drifted out. Occasionally a burst of noise would enter the system (from the YAG and FCL), and a new pattern of 0's and 1's would be stored in the circuit. Figure 3b shows the complementary pattern of pulses obtained when noise causes a section of the pulse train to drop out. These ne patterns were stably held in the circuit until the next noise burst. Figure 4a shows the edge of a rectangular pulse train, to show that all pulses were either unswitched or fully switched. No half-switched pulses were observed. This rectangular pulse train has a rise time, then, which is close to the half width of the 15 ps pulses which were used to drive the system. The circuit functioned over a wide range of signal powers (18 - 60 mW coupled into the fiber from the FCL) due to the heavy saturation of the EDFA. The gain of the EDFA was always between 10 and 20. Stable behavior was observed as the output power of the amplifier was varied over a wide range (45 - 70 mW) with 35 mW of signal light coupled into the fiber.

The contrast at the transmission after adjusting the polarization controllers (Figure 4b) was better than could be measured from the scope photograph. Without adjusting the power or the controllers to the system, the observed contrast at any port was 10:1 or better. The stability of this system is due in part to the digital nature of the switching function [6], but also to the use of birefringent slip in the polarization maintaining fiber to absorb timing jitter[7]. The graph in Figure 5 shows the effects of changing the delay between the signal and control pulse on the transmission of the 1's at TO. The transmission of the 1's (the signal at TO divided by the signal at MON) is essentially independent of the timing over a range of approximately 100 ps. This agrees extremely well with the value of 96 ps from the averaged walkoff times of the cross-spliced sections in the loop.

This experiment demonstrates that the switching function provided by a nonlinear Sagnac loop interferometer is sufficient to build an infinitely cascadable system. The excellent contrast and true binary behavior of the device exhibited in this experiment using 15 ps pulses indicate that it may be possible to perform cascadable logic operations at rates which exceed those of electronic circuits. This is made possible in large part due to the immunity of the system to pulse shape and the tolerance of the system for timing jitter, which is extremely important in an ultrafast system. The ability of the system to hold its state demonstrates a simple fiber loop memory, and also a rudimentary finite state machine. This result suggests that more complicated optical circuits are possible.

1. K. Otsuka, Opt. Lett. 8, 471 (1983).
2. M. Jinno and T. Matsumoto, 13C-16, 1990 Int Top. Mtg. Phot. Sw., Kobe, Japan, 1990.
3. A. Takada, K. Aida and M. Jinno, TuN3, OFC, 1991.
4. K. J. Blow, N. J. Doran, and B. P. Nelson, Elec. Lett., **26**, 962 (1990).
5. K. J. Blow, N. J. Doran, B. K. Nayar, and B. P. Nelson, Opt. Lett., **15**, 248, (1990).
6. H. Avramopoulos, P.M.W. French, M.C. Gabriel, H. H. Houh, N.A. Whitaker, Jr., T. Morse, IEEE Phot. Tech. Lett. 3, 235 (1991).
7. N. A. Whitaker, Jr., H. Avramopoulos, P.M.W. French, M.C. Gabriel, R. E. LaMarche, D. J. DiGiovanni, H. M. Presby, submitted to Opt. Lett.
8. J. D. Moores, K. Bergman, H. A. Haus and E. P. Ippen, JOSA B8, 594 (1991).

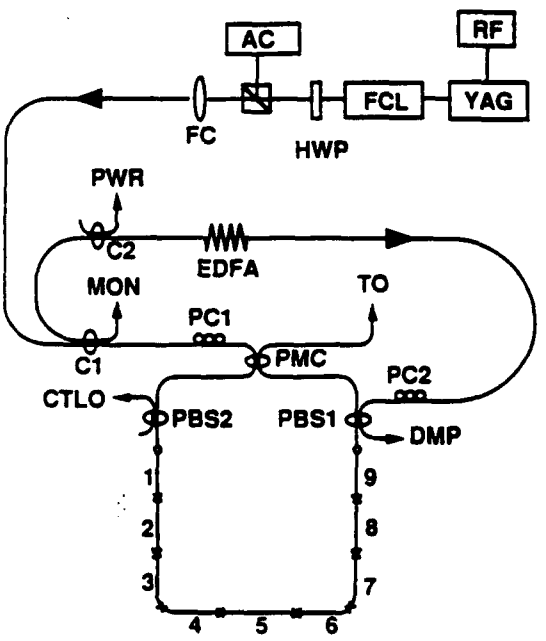

Figure 2: Experimental schematic.

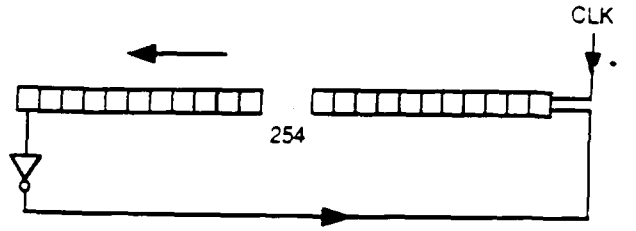

Figure 1: Logical schematic of experiment showing 254 bit clocked shift register and inverted feedback.

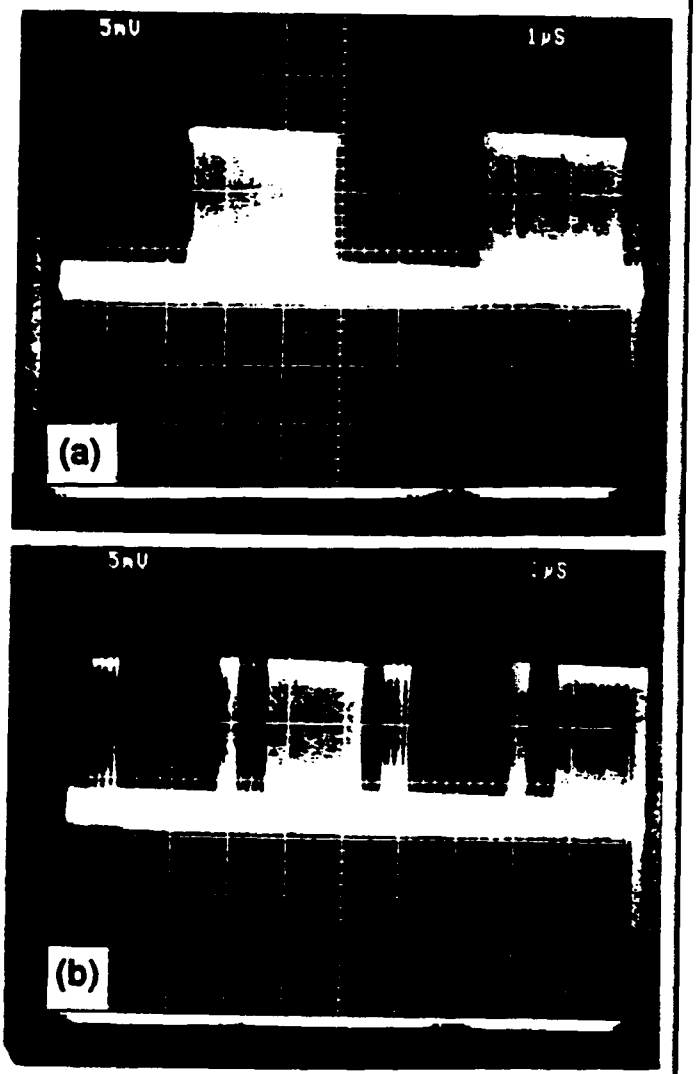

Figure 3: a) CNTLO output starting from an initial condition of all 0's. b) Shift register output starting from a mixed initial condition.

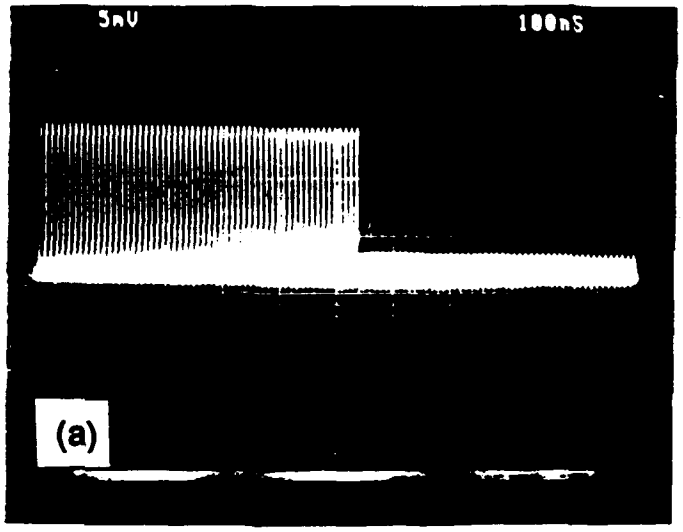

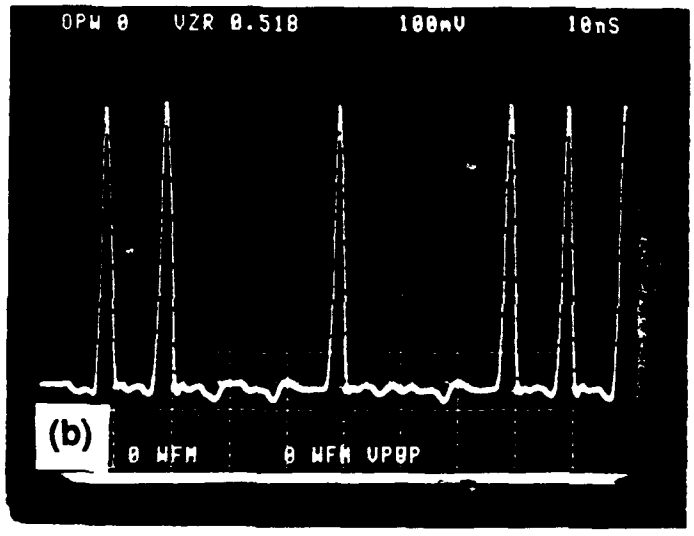

Figure 4 : a) CNTLO output showing the binary nature of the pulse train at the transition. b) TO output showing the high contrast in transmission.

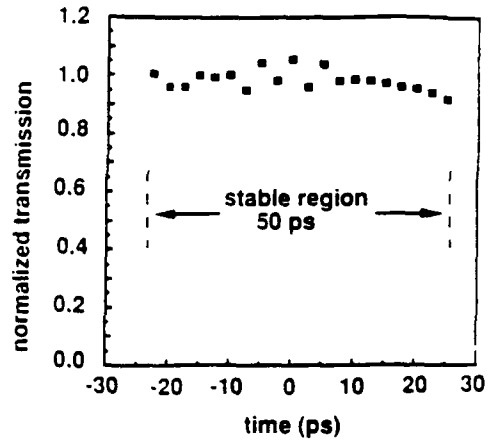

Figure 5: Normalized transmission v timing adjustment showing the constant heig of the 1's as the timing is varied over the st window.

All-optical analog-to digital and digital-to analog conversion based on cross-phase modulation

J.-M. Jeong and M.E. Marhic

Department of Electrical Engineering and Computer Science

Northwestern University

2145 N. Sheridan Rd., Evanston, IL 60208

Phone: (708) 491 7074

Because of the increased use of fiber-optic sensors and fiber-optic communications, signals applied to an optical signal processor are often optical, and thus optical A/D and D/A converters should handle optical input signals directly and be very fast. Optical A/D conversion has been demonstrated and proposed using an electro-optic waveguide [1], a liquid crystal device [2], and optical logic and a look-up table [3]. Optical D/A converters have also been proposed and demonstrated using electro-optic waveguide. Papuchon et al. [4] and Lewis et al. [5] used binary weighted electrodes and binary weighted neutral density filter arrays, respectively.

We propose a technique of ultra-fast nonlinear processing that performs A/D and D/A conversion entirely in the optical domain. The basic principle of operation is based on cross-phase modulation (XPM) between a pump and a signal of different wavelengths due to the optical Kerr effect. The fundamental component of all-optical A/D and D/A converters is a fiber-optic Mach-Zehnder interferometer, as shown in Fig. 1 (a). In the absence of the pump, the interferometer is balanced at the wavelength of the probe. In the presence of the pump, the interferometer becomes unbalanced via cross-phase modulation due to the optical Kerr effect, and the output power is given by

$$P_o = P_s \sin^2(\frac{\Delta\Phi}{2}), \tag{1}$$

where P_s is the power of the probe and $\Delta\Phi$ is nonlinear phase shift. $\Delta\Phi$ is given by

$$\Delta\Phi = Q\int_0^L P_p[t - (\frac{1}{v_{g1}} - \frac{1}{v_{g2}})z]dz, \tag{2}$$

where Q is the fiber nonlinear coefficient, $P_p(t)$ is the pulse shape of the pump pulse, and L is the interaction length. v_{g1} and v_{g2} are the propagation velocities of the probe and the pump, respectively.

A/D conversion. If an optical analog signal is used as an input pump in Fig. 1, we can implement A/D conversion. As shown in Eq. (1), the output powers vary sinusoidally as the pump power is increased. This periodic dependence is the basis of an A/D converter. When the interaction length is small compared with the pulse walk-off length, $\Delta\Phi$ is proportional to the pump power $P_p(t)$ and the interaction length L, i.e. $\Delta\Phi = QP_p(t)L$. If the modulator interaction length or the pump power differ by a factor of 2 between bits, we can generate Gray codes by combining the interferometers in parallel. In this converter, if we use a pulsed laser for the probe, sampling of the analog input signal can be accomplished. The repetition rate of the pulsed laser will be the sampling frequency.

D/A conversion. The basic configuration of an all-optical 3-bit D/A converter is shown in Fig. 1 (b). The interaction lengths are L, $2L$, and $4L$ for bit 0, bit 1, and bit 2, respectively. The pump pulses are used

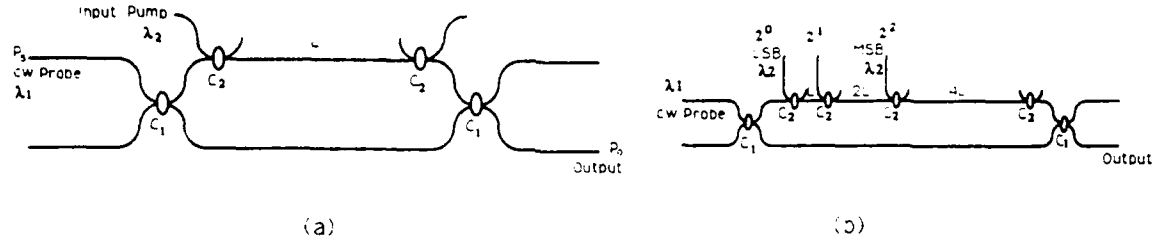

Figure 1: (a) The fundamental component of A/D and D/A converters. (b)The basic configuration of 3-bit D/A converter. C_1=3dB coupler; C_2=WDM coupler.

for the applied digital word. When the interaction length is small compared with the pulse walk-off length , the total nonlinear phase shift, $\Delta\Phi_{tot}$ is given by

$$\Delta\Phi_{tot} = QP_p(t)\sum_{n=1}^{3} a_n 2^{n-1} L, \tag{3}$$

where a_n = 1 or 0 depending on the digital bit. Thus, $\Delta\Phi_{tot}$ represents the analog value of the digital word. Since the output power is proportional to $sin^2(\Delta\Phi/2)$, the ouput of the proposed D/A converter does not exactly represent the analog value of the applied digital word. However, by limiting the pump power and applying an appropriate bias, we could obtain almost linear response.

The experimental setup is shown in Fig. 2. To reduce environmental phase fluctuations, we used a Sagnac interferometer instead of the proposed Mach-Zehnder interferometer. For the pump pulses, we used a frequency-doubled Nd:YAG laser at the wavelength of 532nm, repeatedly Q switched at 1-5kHz, producing pulses with 100-200 W peak power. Pulse lengths were 150nsec fwhm. For the probe, a cw He-Ne laser was used, operating at the wavelength of 633nm. The power coupling ratio of the WDM coupler was 99% at 532nm and 5% at 633nm. The excess loss was less than 0.2dB. BS1, BS2, single-mode fiber loop and WDM coupler constitute a Sagnac interferometer. We used a red filter to separate the pump and the signal at the output of the fiber loop. In a typical experiment, we adjusted the optics to obtain a high-contrast interference pattern for the CW probe and located the photomultiplier tube at the dark fringe. Here because of the long pump pulse, the pulse walk-off length is much longer than the interaction length.

For A/D conversion, we used the input B only, blocking the input A, and varied the power of the analog input pump by a factor of 2 instead of the interaction length. The interaction length was 200m. The modulated outputs for the falling half of the pump pulse are shown in Fig. 3. Fig. 3(a), (b), and (c) are the output of the MSB, $NLSB$, and LSB when the peak pump powers were 0.39 W, 0.77 W, and 1.55 W, respectively. The solid lines are the theoretically predicted outputs and the squares are the measured data points. As shown in Fig. 7, the maximum nonlinear phase shifts are π, 2π, and 4π for the MSB, $NLSB$, and LSB, respectively. The theoretically calculated value of the pump power for a π phase shift is 0.4 W when the interaction length is 200m long. Fig. 3(d) shows the corresponding reconstructed output from the measured 3-bit Gray codes. The dotted line is the shape of the falling half of the input pump and the squares are the calculated points from the measured data, assuming that the threshold of the comparator is at $P_s/2$.

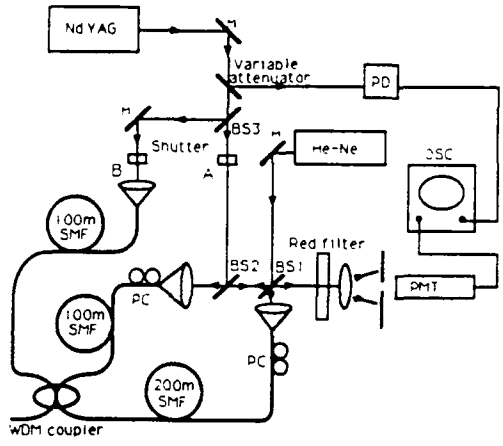

Figure 2: Experimental setup for 3-bit A/D and 2-bit D/A converters

For D/A conversion, we demonstrated the 2-bit D/A converter. We used the input A and B for the 2^0 bit and 2^1 bit, respectively. Interaction lengths are 100m and 200m for the 2^0 bit and 2^1 bit, respectively. Fig. 4 shows the outputs when the 2-bit digital words applied to the interferometer are 00, 01, 10, and 11, respectively. The bit values 0 and 1 are equal to 0W and 0.13W of the peak power of the input pump pulse, respectively. The nonlinear phase shifts were 0π, $1/3\pi$, $2/3\pi$, and π for the input digital word 00, 01, 10, and 11, respectively.

In conclusion, we have proposed and demonstrated all-optical A/D and D/A conversion in a two-wavelength single-mode fiber optic interferometer. The technique has many advantages relative to other conversion approaches. First, the proposed converter can be used directly with optical input signals, unlike in the electro-optic waveguide approach. The output of the device can also be optical. The all-optical technique can be very fast because of the inherent speed of the optical Kerr effect. Finally, the device is relatively simple because it requires no electronic circuits and other optical components. The concept can in principle be extended to single-wavelength operation by using cross phase modulation between two orthogonally polarized waves. The A/D converter demonstrated here supposes the existence of a fast threshold device, which has yet to be developed. The high speed D/A converter can be useful in the generation of various shapes of wideband analog waveforms.

References

[1] R. A. Becker, C. E. Woodward, F. J. Leonberger, and R. C. Williamson, *IEEE Proc.*, **72**, pp.802-819, 1984.

[2] A. Armand, A. A. Sawchuck, T. C. Strand, D. Boswell, and B. H. Soffer, *Opt. Lett.*, **5**, pp.129-131, 1980.

[3] A. D. McAulay, *Opt. Eng.*, **29**, pp.114-120, 1990.

[4] M. Papuchon, C. Puech, and A. Schnapper, *Electron. Lett.*, **16**, pp.142-144, 1980.

[5] M. F. Lewis and C. L. West, *Electron. Lett.*, **25**, pp.200-202, 1988.

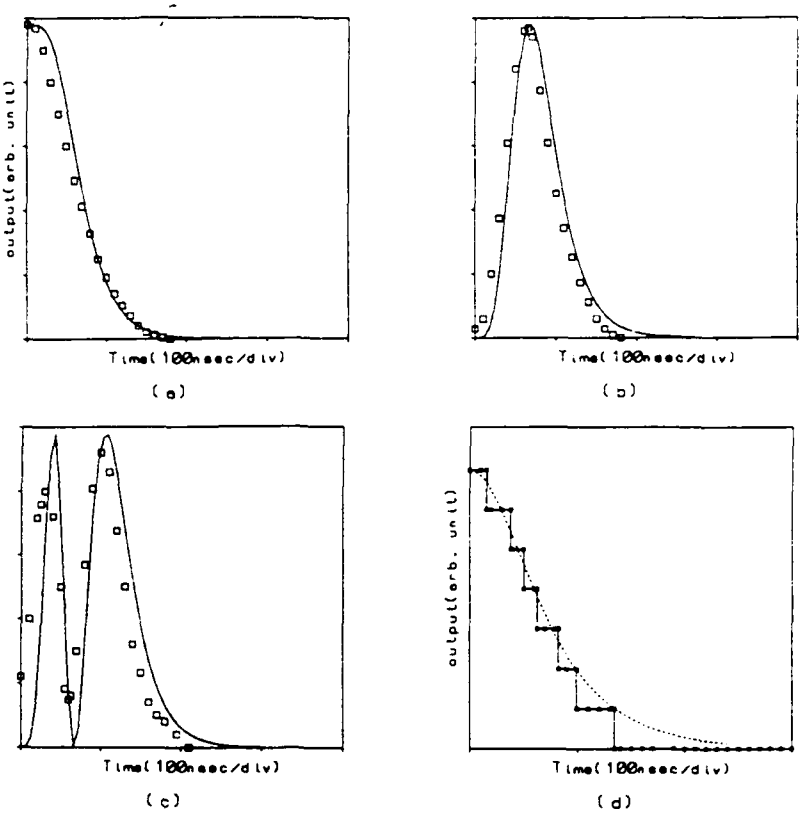

Figure 3: Experimental data: (a) bit 0, (b) bit 1, and (c) bit 2. Solid lines are theoretically predicted outputs. Squares are the measured data. (d) The reconstructed output, assuming the detection threshold at $P_s/2$.

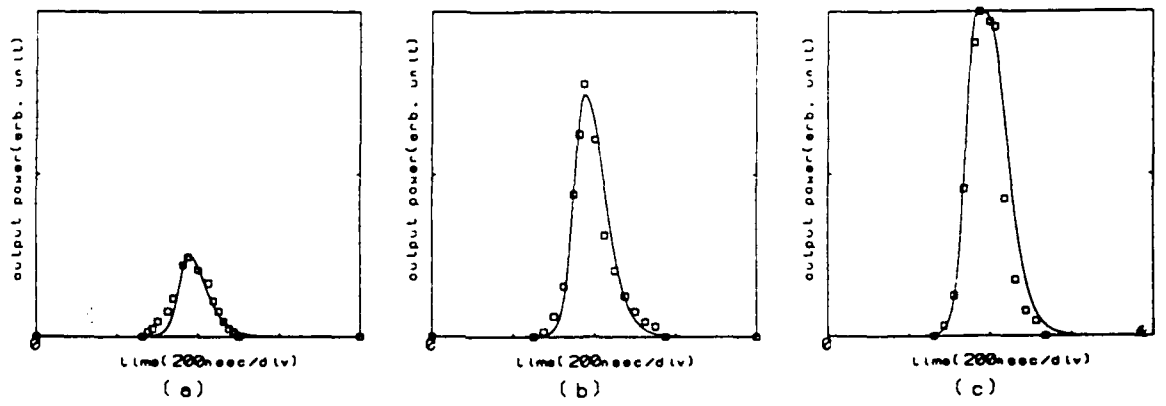

Figure 4: Experimental data: Outputs for the input digital words (a) 01, (b) 10, and (c) 11.

Key to authors

Afanasjev, V. V. - Pd1

Andreadakis, N.C. - Pd4
Aitchison, J. S. - Pd2
Avramopoulos, H. - Pd11

Blouin, Alain - Pd6

Chase, E. W. - Pd7
Colas, E. - Pd4

da Silva, V. L. - Pd7
Doran, N. J. - Pd10

Finlayson, N. - Pd13

Gabriel, M. C. - Pd11
Grant, R. S. - Pd4
Grudinin, A. B. - Pd8

Heritage, J. P. - Pd7
Hobson, W. S. - Pd3
Huang, A. - Pd11

Ironside, C. N. - Pd2
Islam, M. N. - Pd3

Jeong, J.-M. - Pd12

Kean, A. H. - Pd2
Kimura, Yasuo - Pd9

LaRochelle, Sophie - Pd6
LeBlanc, H. P. - Pd4
Levi, A. F. J. - Pd3

Marhic, M. E. - Pd12

Nakazawa, Masataka - Pd9
Nayar, B. K. - Pd10

Ouellette, Francois - Pd6

Payne, D. N. - Pd8
Penty, R. V. - Pd4
Poole, Simon B. - Pd5

Richardson, D. J. - Pd8

Sceats, Mark G. - Pd5
Sibbett, W. - Pd4
Silberberg, Y. - Pd7
Slusher, R. E. - Pd3
Soccolich, C. E. - Pd3
Stegeman, G. I. - Pd2

Tsang, H. K. - Pd4

Villeneuve, A. - Pd2
Vysloukh, V. A. - Pd1

Whitaker, N. A. - Pd11
White, I. H. - Pd4

Yoshida, Eiji - Pd9
Young, M. G. - Pd3